Dual-Motor Control for Backlash Reduction in Parallel-Kinematic Robot Joints

Mathias Artursson

LUND UNIVERSITY

Department of Automatic Control

MSc Thesis
TFRT-6086
ISSN 0280-5316

Department of Automatic Control
Lund University
Box 118
SE-221 00 LUND
Sweden

Printed in Sweden by Tryckeriet i E-huset
Lund 2019

Abstract

A new high-performance robot called the Gantry-Tau robot was developed by ABB Robotics, the Robotics Lab at Lund University and Güdel AG. This robot seemed promising in terms of speed, accuracy, stiffness and bandwidth of the motion control. However, the robot joints were based on the rack-and-pinion principle, which introduced significant backlash into the system. To solve this problem, it was proposed to use two motors to control each joint, where the motors would go in opposite directions to ensure that the gears and motors were in contact at all times. How this should be implemented is still under development.

This master thesis attempted to implement backlash compensation together with conventional uses of the robot joints, such as position-, velocity- and acceleration-trajectories as well as torque feed forward. The goal for the cart was to have regular control for both motors when following trajectories, except for stationary points where the motors would work in different directions. A test rack was provided for this purpose by Lund University and Cognibotics.

First, trajectories were generated for the robot joint to follow. A control structure was then implemented for the robot joint, consisting of a cascade structure for position control, as well as torque feed forward from a friction and dynamic model. Different methods for backlash-compensation were also presented and implemented. These methods for backlash-compensation together with the control structure were then evaluated in terms of position accuracy without external disturbances, and overshoot, settling time and backlash traversal with external disturbances.

It was concluded that some implemented backlash compensation methods resulted in a more dampened response when no external disturbances were present. Experiments with external disturbances showed that performance could be improved in some situation, but became worse in others. The reason for this decreased performance may have been because the controlling motor went through the backlash gap.

Acknowledgements

This master thesis was done in collaboration with Cognibotics and the Department of Automatic Control at Lund University. I would like to thank the following people who contributed to this master thesis in some form:

- The CEO at Cognibotics, Klas Nilsson, for giving me the opportunity to do my master thesis at his company. It has been very interesting to gain insight in how you work and being able to use the test rack.
- My supervisors Anders Robertsson at Lund University and Olof Sörnmo at Cognibotics, for giving me a crash course in robotics as well as tips and feedback.
- My examiner Rolf Johansson at Lund University, for suggesting Cognibotics as a potential company to do my master thesis at.
- My student thesis opponents and friends Eric and Christian for giving me feedback.
- My girlfriend, mother, sister and brother for their love and support throughout the process.
- My friends and classmates for their tips as well as for their lunch- and coffee breaks.

Contents

1

Introduction

1.1 The parallel-kinematic Gauntry-Tau robot

Within the EU FP-6 project SMErobot™, a new high-performance robot was developed by ABB Robotics, the Robotics Lab at Lund University and Güdel AG [SMErobot, 2009]. The robot, which is called the Gauntry-Tau robot, can be seen in Figure 1.1. The concept was based on a non-redundant parallel configuration of the robot joints. The three carts were controlled along its rails to move a tool along a desired trajectory. This concept allowed for an easily scalable modular system with a large open work space. The joints and arms also had high stiffness and low inertia. All of this combined made it possible to build high-performance robots with respect to speed, accuracy, stiffness and motion control bandwidth. Especially the high motion control bandwidth of the robot made it very suitable for stiff contact force control tasks. Possible applications were laser, water and plasma jet cutting, grinding, gluing and assembly [Halt, 2009, pg.1] [Schiffer, 2009, pg.1-2].

1.2 Problem formulation

The robot joints seen by Figure 1.1 were based on the rack-and-pinion principle, which is illustrated in Figure 1.2. This lead to backlash in both the gearbox and in the connection to the rail, which compromised position accuracy and stiffness of the robot joint. To achieve high performance from the robot, then these effects needed to be compensated for.

An idea which has been developed within the SMErobot™ project, was using two motors to control each cart, instead of using only one motor for each cart. The idea was for the motors to work in opposite directions, which is illustrated in Figure 1.3. This way, one motor would act as a spring and close the backlash gap in the connection to the rail. However, it would be very energy inefficient to have the second motor work against the first one at all times. It was therefore of interest to investigate how the second motor should transition from regular control to working in opposite direction as the first motor.

Figure 1.1 Gantry-Tau prototype, where the three orange carts were controlled along their rails to move a tool along a desired trajectory [SMErobot, 2009].

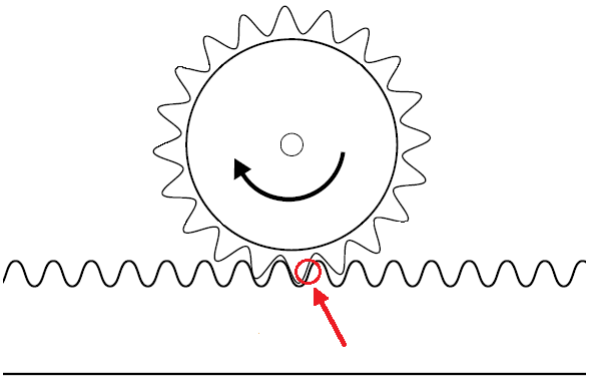

Figure 1.2 Rack-and-pinion principle, where backlash occurs in the connection to the rail.

There have been previous master theses within this area. The ones that this master thesis primarily worked with were [Schiffer, 2009], [Halt, 2009] and [Cairén, 2013].

In [Schiffer, 2009], it was mathematically shown that limit cycles were introduced due to the backlash gap, and that these were removed by the introduction of the second motor working in the opposite direction as the first one. In [Schiffer,

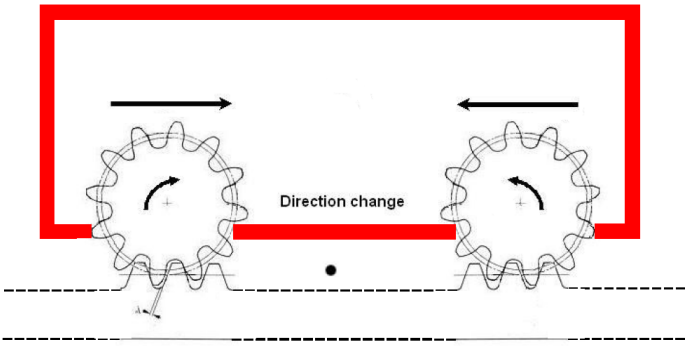

Figure 1.3 Two motors working in opposite directions to close the backlash gap in the connection to the rail [Schiffer, 2009, pg.4].

2009], simulations also showed that using two integral action parts in parallel resulted in unstable behaviour, which was problematic considering that two motors were to be controlled. Two possible solutions were proposed, where the first solution was to only have integral action on one of the motors, and the second solution was to have one integral action part distributed among both motors.

In [Halt, 2009], a similar control structure was implemented as in [Schiffer, 2009]. [Halt, 2009] also constructed a workbench involving encoders, a digital signal controller and power electronics. This was then used to evaluated stiffness of the cart control.

In [Cairén, 2013], a dual-motor control platform was made, and a control strategy was also implemented,

Both [Schiffer, 2009] and [Halt, 2009] based their control structures on the first proposed solution mentioned in [Schiffer, 2009], where only one motor had integral action for angular velocity control. Performance was also investigated using three switching strategies which were based on either position error, relative position angle of motor and load, or both. Both [Schiffer, 2009] and [Halt, 2009] concluded that using a switching strategy based on using only position error yielded the overall best results. In [Cairén, 2013], the control structure was instead based on the second proposed solution mentioned in [Schiffer, 2009], where one integral action part was distributed among both motors. Performance was also investigated using a switching strategy which was based on the velocity control signal, and made it so that one motor went in the opposite direction at all times. The implementations of the systems in [Schiffer, 2009] and [Halt, 2009] were also based on position step responses, while the use of trajectories were incorporated in [Cairén, 2013].

This master thesis continued previous work, by attempting to implement switching strategies to more conventional uses of the robot joints, such as position-, velocity- and acceleration-trajectories as well as torque feed forward. The second

solution proposed in [Schiffer, 2009] was also implemented, which was to use one integral action part distributed among both motors. Continued investigations were also made on previous successful switching strategies in [Schiffer, 2009] and [Halt, 2009], as these switching strategies had the benefit of being more energy efficient than the switching strategiy used in [Cairén, 2013].

The goal was for the cart to have regular control for both motors when following trajectories, except for stationary points where the motors would work in different directions. This master thesis only investigated this transition as stationary position points were approached. Both motors also always started in contact with the gears in the beginning of all experiments.

1.3 Outline

First, the test rack used for this master thesis is presented in Chapter 2, as well as an analysis of the backlash gap sizes for the system.

The trajectories for the cart are presented in Chapter 3. Here, two trajectories for going to a final position reference were derived, which served as a foundation for this master thesis by being equivalent to a position step response. In addition to these two trajectories, a cosine trajectory was also derived to investigate more dynamic properties of the system.

The control structure and torque feed forward without backlash compensation i.e., when both motors work identically, are presented in Chapter 4. Here, the velocity and position control was derived, as well as a friction- and dynamic model. A brief evaluation of single motor control was also made.

Switching strategies for motor 2 are presented in Chapter 5.

An experimental evaluation is presented and discussed in Chapter 6. Here, performance with and without disturbances were evaluated.

A discussion about the master thesis is then presented in Chapter 7

Conclusions as well as possible future work are finally presented in Chapter 8.

2

Test rack

For this master thesis, a test rack was provided by the Robotics Lab at Lund University and Cognibotics. The test rack can be seen in Figure 2.1, and a closer look at the cart that was controlled can be seen in Figure 2.2.

2.1 DC motors

The cart was equipped with DC-motors. An electric circuit for a DC-motor can be seen in Figure 2.3.

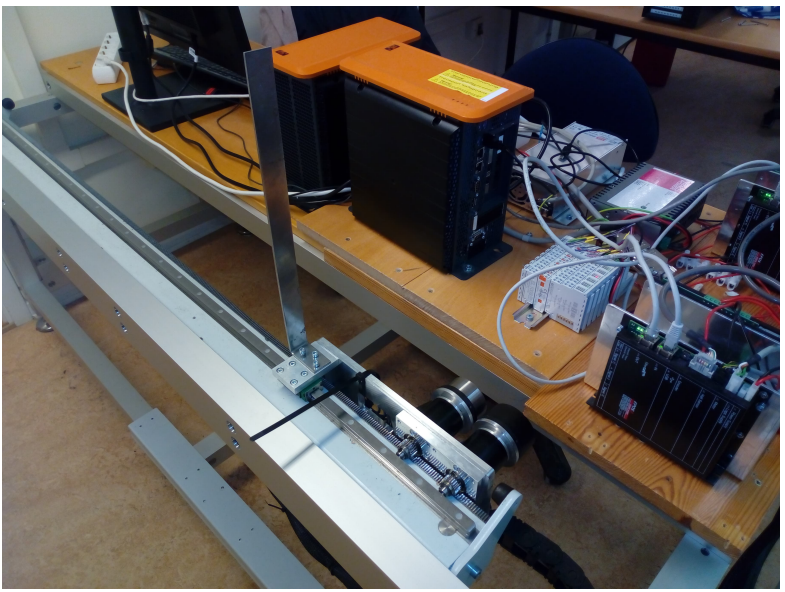

Figure 2.1 The test rack used.

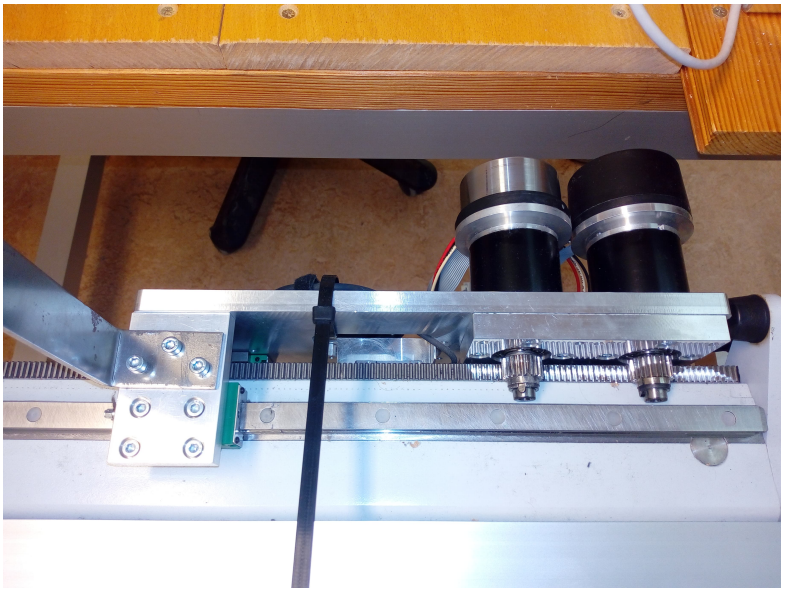

Figure 2.2 The joint that is to be controlled i.e., the position of the cart along the rail. The motor to the left was motor 1 and the one to the right was motor 2.

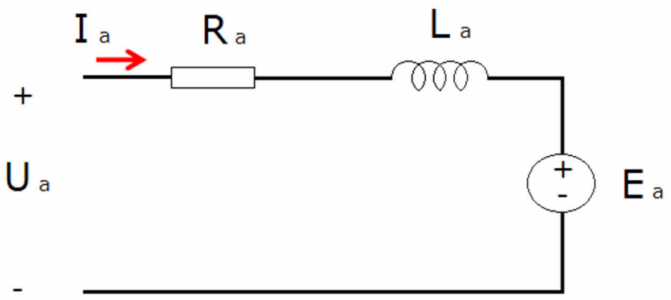

Figure 2.3 An electric circuit for a DC-motor. U_a [V] is armature voltage, I_a [A] current, R_a [Ω] resistance, L_a [H] inductance and E_a [V] induced back emf in the motor.

In a DC-motor, torque is proportional to armature current. However, back emf is proportional to motor speed [Marquez and Domingues, 2010, pg.13]. Due to outer disturbances and the induced back emf, the armature current (or voltage) is needed to be controlled for desired motor torque. Subsequently, when a torque reference was set by the user for the motors on the test rack, then a corresponding current reference was set and controlled internally by the system.

2.2 System information

- The sample time was $h = 1$ ms.
- The cart was equipped with a linear encoder, where $s_{mm/lin} = 1.953727 \cdot 10^{-5}$ [mm/linear encoder tick].
- The motors were equipped with rotary encoders, which had $N_{motor} = 16384$ counts per revolution, and where $s_{mm/mot} = 3.131442945 \cdot 10^{-4}$ [mm/motor encoder tick].
- The gear ratio for the gearbox was $N_{gear} = 20$.
- The absolute maximum torque a motor can be subjected to was $u_{max} = 316.92$ [Nm].
- The torque references and torque measurements were in promilles of the maximum torque i.e., had the unit [316.92 mNm].
- The absolute maximum velocity using both motors was approximately $v_{max} = 288$ [mm/s].

The inputs/outputs used to communicate with the system can be seen in Table 2.1. Full system implementation for TwinCat3 can be found in the GitLab repository: `git@gitlab.control.lth.se:Robertsson/exjobb_DualMotor_Artursson_VT2019.git`.

2.3 Backlash gap size analysis

Here, an analysis of the size of the backlash gap in the system was made, as it gave insightful information how the backlash affected the system. This analysis could be made because the cart was equipped with a linear encoder, and the motors with rotary encoders. When the cart moved through the gap, it was expected that the motors rotate without the cart moving. This meant that the rotary encoders were

Table 2.1 Inputs/outputs used for the test rack.

Name	I/O	Variable type	Unit
Measured torque motor 1	Input	INT	316.92 mNm
Measured torque motor 1	Input	INT	316.92 mNm
Cart position	Input	UDINT	$1.953727 \cdot 10^{-5}$ mm
Motor 1 position	Input	DINT	$3.131442945 \cdot 10^{-4}$ mm
Motor 2 position	Input	DINT	$3.131442945 \cdot 10^{-4}$ mm
Torque reference motor 1	Output	INT	316.92 mNm
Torque reference motor 2	Output	INT	316.92 mNm

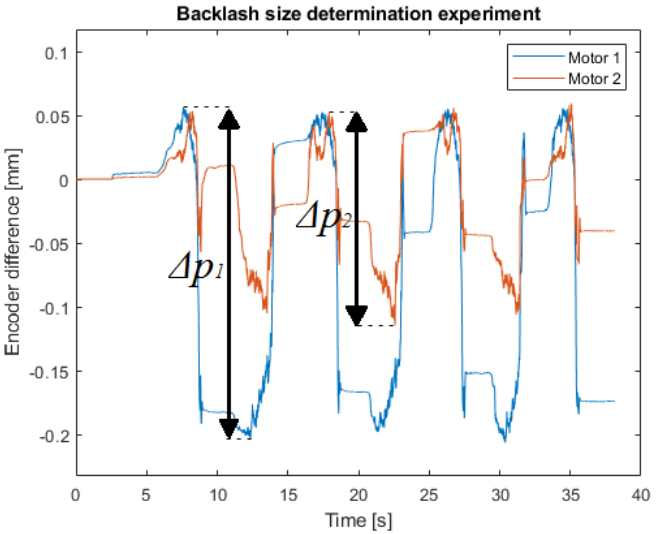

Figure 2.4 Plot of differences between the rotary encoders and the linear encoder. The cart was pushed back and forth, whilst the torque references were set to zero. The backlash gap size in terms of length was Δp_1 for motor 1, and Δp_2 for motor 2.

expected to increment their position measurements, but not the linear encoder when the cart moved through the backlash gap. The difference between the position measurements from the rotary encoders and the linear encoder would therefore contain information about the size of the backlash gap.

An experiment was made by recording the difference between these encoders as the cart moved. An example of how this could be done was by pushing the cart back and forth, where the motors have their torque references set to zero. Results from this experiment resulted in Figure 2.4.

From results seen in Figure 2.4, the effect of the backlash gap in terms of position for motor 1 and motor 2 could be approximated to $\Delta p_1 = 256.9$ [μm] and $\Delta p_2 = 163.4$ [μm], respectively.

Assuming that Δp was a result of only the backlash in the connection to the rail, and not within the gearbox itself, then the backlash size α [°] could be calculated according to Eq. (2.1)

$$\alpha = 360^\circ \frac{\Delta p \cdot 10^{-3}}{s_{mm/mot} N_{motor} N_{gear}}. \tag{2.1}$$

Inserting Δp_1 and Δp_2 into Eq. (2.1) resulted in the backlash angles $\alpha_1 = 0.9013^\circ$ and $\alpha_2 = 0.5733^\circ$ for motor 1 and motor 2 respectively.

Note that this result is only locally valid in one region of the rack, as the size of

the backlash gap may vary. The presented results of measuring Δp and α are rather to give insight in the approximate magnitude of the backlash gap and its effects on position uncertainty.

3

Trajectories

This master thesis worked on improving trajectory position accuracy and stiffness at stopping points. The used trajectories for this purpose are presented below. Throughout this section, the approximation $t = (k-1)h$ was made, where t [s] is time and k the sample number.

3.1 Step trajectory

The simplest trajectory is probably one used for going from one point from another. Therefore, improving accuracy using this trajectory would serve as foundation for this master thesis. Inspiration for this section was from [Linderoth, 2013, pg.87-111].

A simple way this trajectory could be generated was by assuming piece-wise constant acceleration. Using this approach, the derivative of the acceleration, called jerk, would (theoretically) be infinite at time points where the acceleration changed values. This could cause excessive wear on the system, as well as excite mechanical resonances which would reduce performance [Linderoth, 2013, pg.89]. When using a dynamic model shown in Section 4.3, using a sharp acceleration profile also introduced sharp torque fed to the system, which could possibly compromise precision.

An alternative to this could be to instead assume piece-wise constant jerk. Using this approach however would cause the step to become slower as well as greatly increase complexity of the trajectory.

Infinite jerk

In this section, a step trajectory was derived using infinite jerk, which started off as a piece-wise constant acceleration trajectory. The step profile was calculated given a maximum absolute acceleration, velocity and final destination. When using a step profile with a piece-wise constant acceleration trajectory, given a maximum absolute velocity, then two cases could occur, which are if the velocity becomes saturated or not.

Case 1: Unsaturated velocity

If it was desired for the cart to move the distance p_f [mm] given the desired maximum absolute acceleration a_{max} [mm/s^2], then an acceleration trajectory $a_{ijerk1}(t)$, assuming Case 1 for a step trajectory with infinite jerk, could look like according to Eq. (3.1) and Figure 3.1

$$a_{ijerk1}(t) = \text{sign}(p_f) \cdot \begin{cases} a_{max} & \text{if } t_a > t \\ -a_{max} & \text{if } 2t_a > t \geq t_a \\ 0 & \text{if } t \geq 2t_a \end{cases}, \tag{3.1}$$

where t_a [s] was the time with constant acceleration (different from zero). The time t_a was unknown at this point, so an expression for this needed to be derived using p_f and a_{max}. This could be done through further integration.

The velocity profile v_{ijerk1} was received by integration of a_{ijerk1}. Doing so resulted in v_{ijerk1} being according to Figure 3.2 and Eq. (3.2)

$$v_{ijerk1}(t) = \text{sign}(p_f) a_{max} \cdot \begin{cases} t & \text{if } t_a > t \\ 2t_a - t & \text{if } 2t_a > t \geq t_a \\ 0 & \text{if } t \geq 2t_a \end{cases}. \tag{3.2}$$

The position profile p_{ijerk1} was received by integration of v_{ijerk1}. Doing so resulted in p_{ijerk1} being according to Figure 3.3 and Eq. (3.3)

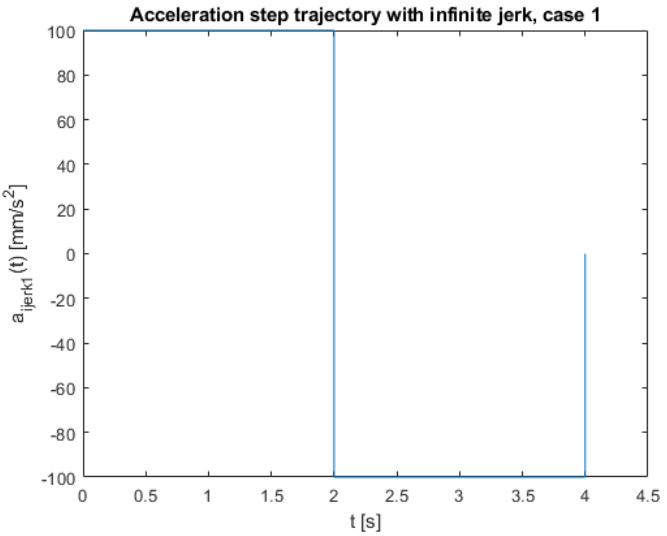

Figure 3.1 Plot of acceleration step trajectory with infinite jerk, Case 1, where $a_{max} = 100$ mm/s^2, $t_a = 2$ s and an assumption that $p_f > 0$.

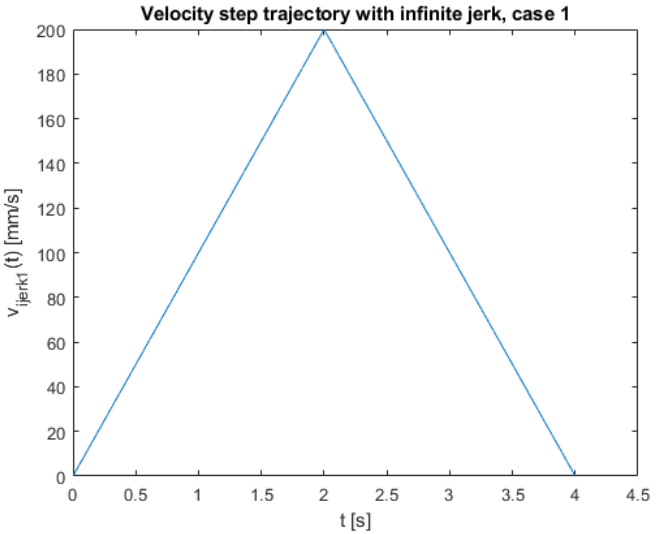

Figure 3.2 Plot of velocity step trajectory with infinite jerk, Case 1, where $a_{max} = 100$ mm/s^2, $t_a = 2$ s and an assumption that $p_f > 0$.

$$p_{ijerk1}(t) = \text{sign}(p_f) a_{max} \cdot \begin{cases} \frac{t^2}{2} & \text{if } t_a > t \\ -\frac{t^2}{2} + 2t_a t - t_a^2 & \text{if } 2t_a > t \geq t_a \\ t_a^2 & \text{if } t \geq 2t_a \end{cases}. \tag{3.3}$$

Since it was known that the endpoint for the trajectory was p_f, then t_a could be solved for using Eq. (3.3) when $t \geq 2t_a$. Doing so resulted in Eq. (3.4)

$$t_a = \sqrt{\frac{|p_f|}{a_{max}}}. \tag{3.4}$$

Case 2: Saturated velocity

If it was instead assumed that the velocity became saturated according to the desired maximum absolute velocity v_{max}, then an acceleration trajectory $a_{ijerk2}(t)$ for a step trajectory with infinite jerk, could look like according to Eq. (3.5) and Figure 3.4

$$a_{ijerk2}(t) = \text{sign}(p_f) \cdot \begin{cases} a_{max} & \text{if } t_a > t \\ 0 & \text{if } t_v + t_a > t \geq t_a \\ -a_{max} & \text{if } t_v + 2t_a > t \geq t_v + t_a \\ 0 & \text{if } t \geq t_v + 2t_a \end{cases}, \tag{3.5}$$

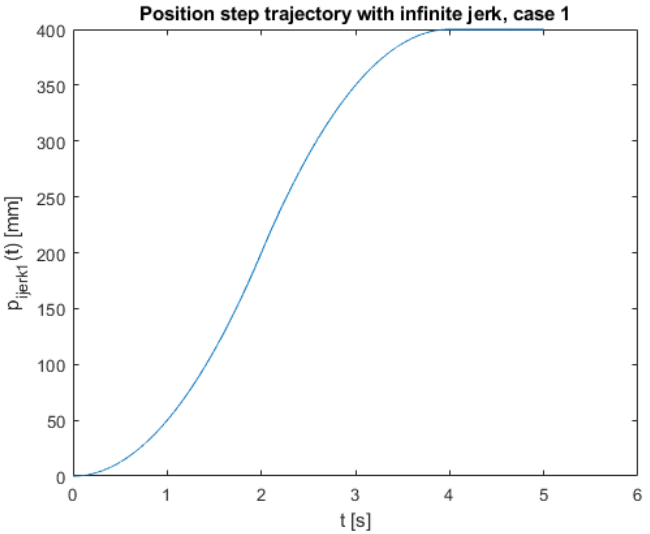

Figure 3.3 Plot of position step trajectory with infinite jerk, Case 1, where $a_{max} = 100$ mm/s^2, $t_a = 2$ s and an assumption that $p_f > 0$.

where t_v [s] was the time with constant velocity (different from zero). An expression for t_a and t_v needed to be derived using p_f, a_{max} and v_{max}. This could once again be done through integration.

The velocity profile v_{ijerk2} was received by integration of a_{ijerk2}. Doing so resulted in v_{ijerk2} being according to Figure 3.5 and Eq. (3.6)

$$v_{ijerk2}(t) = \text{sign}(p_f)a_{max} \cdot \begin{cases} t & \text{if } t_a > t \\ t_a & \text{if } t_v + t_a > t \geq t_a \\ t_v + 2t_a - t & \text{if } t_v + 2t_a > t \geq t_v + t_a \\ 0 & \text{if } t \geq t_v + 2t_a \end{cases}. \tag{3.6}$$

The position profile p_{ijerk2} was received by integration of v_{ijerk2}. Doing so resulted in p_{ijerk2} being according to Figure 3.6 and Eq. (3.7)

$$p_{ijerk2}(t) = \text{sign}(p_f)a_{max} \cdot \tag{3.7}$$
$$\begin{cases} \frac{t^2}{2} & \text{if } t_a > t \\ t_a(t - \frac{t_a}{2}) & \text{if } t_v + t_a > t \geq t_a \\ -\frac{t^2}{2} + t(t_v + 2t_a) - t_a^2 - t_a t_v - \frac{t_v^2}{2} & \text{if } t_v + 2t_a > t \geq t_v + t_a \\ t_a(t_a + t_v) & \text{if } t \geq t_v + 2t_a \end{cases}$$

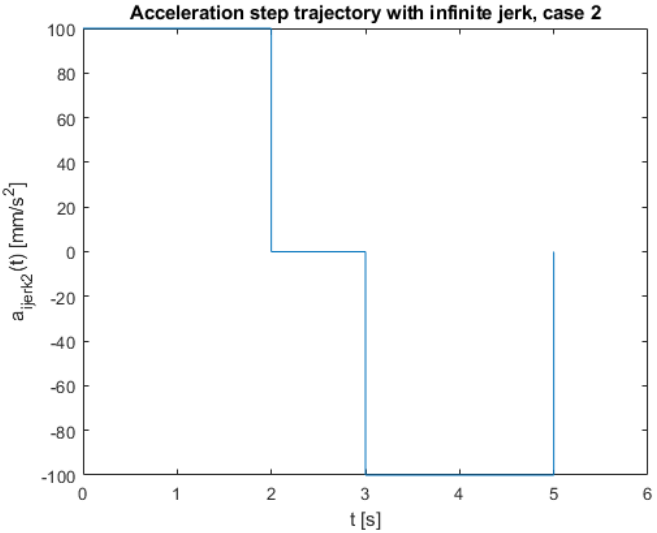

Figure 3.4 Plot of acceleration step trajectory with infinite jerk, Case 2, where $a_{max} = 100$ mm/s^2, $t_a = 2$ s, $t_v = 1$ s and an assumption that $p_f > 0$.

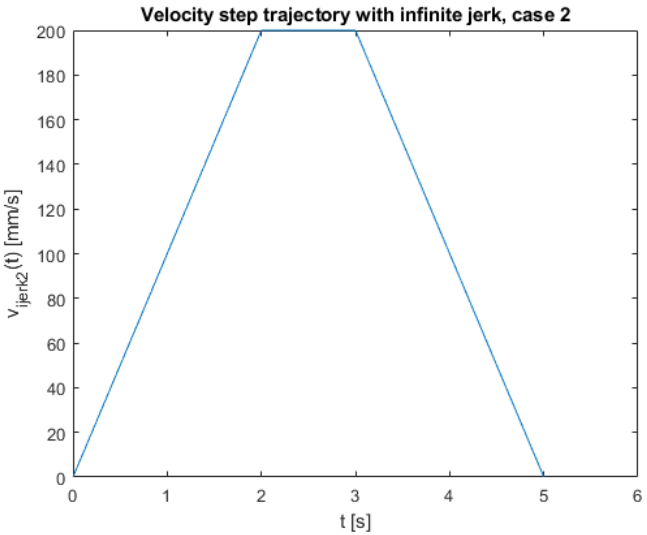

Figure 3.5 Plot of velocity step trajectory with infinite jerk, Case 2, where $a_{max} = 100$ mm/s^2, $t_a = 2$ s, $t_v = 1$ s and an assumption that $p_f > 0$. This resulted in the maximum velocity being $v_{max} = 200$ mm/s.

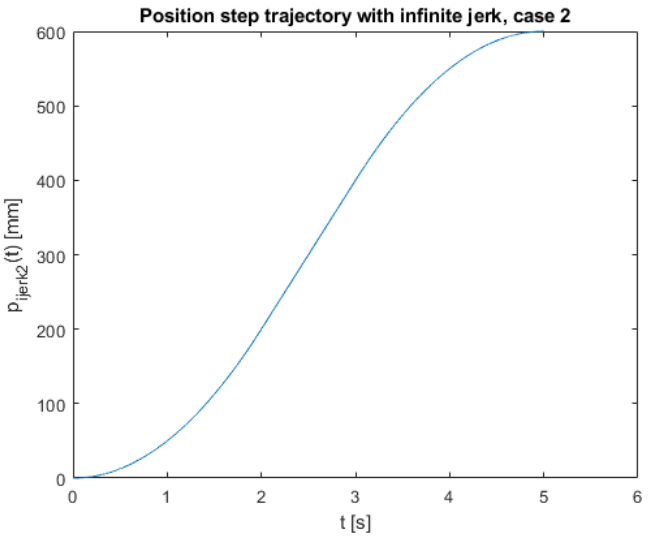

Figure 3.6 Plot of position step trajectory with infinite jerk, Case 2 (saturated velocity), where $a_{max} = 100$ mm/s^2, $t_a = 2$ s, $t_v = 1$ s and an assumption that $p_f > 0$.

Since it was known that the endpoint was p_f and that the velocity saturated at v_{max}, then t_a and t_v could be solved for using Eq. (3.6) when $t_v + t_a > t \geq t_a$ and Eq. (3.7) when $t \geq t_v + 2t_a$. Doing so resulted in Eqs. (3.8) and (3.9)

$$t_a = \frac{v_{max}}{a_{max}}, \tag{3.8}$$

$$t_v = \frac{|p_f| a_{max} - v_{max}^2}{v_{max} a_{max}}. \tag{3.9}$$

Case selection

Given p_f, a_{max} and v_{max}, it was needed to know which case to select for the step trajectory. Since t_v represented the time at which the velocity was constant (different from zero) i.e., when the velocity was saturated, then it sufficed to look at the sign of t_v in Eq. (3.9). The case was selected as follows.

- Case 2: If $t_v \geq 0$ for t_v in Eq. (3.9)
- Case 1: Otherwise

When the case had been determined, then the acceleration, velocity and position trajectories to the corresponding case were initialised and used to control the cart.

Finite jerk

In this section, a step trajectory was derived with finite jerk, using a piece-wise constant jerk trajectory. The step profile was calculated given a maximum absolute jerk, acceleration, velocity and final destination. When using a step profile with a piece-wise constant jerk, given a maximum absolute acceleration and velocity, then four Cases could occur: unsaturated velocity and acceleration, unsaturated velocity and saturated acceleration, saturated velocity and unsaturated acceleration and finally saturated velocity and acceleration.

Case 1: Unsaturated velocity, unsaturated acceleration

If it was desired for the cart to move the distance p_f [mm] given the desired maximum absolute jerk j_{max} [mm/s^3], then a jerk trajectory $j_{fjerk1}(t)$, assuming Case 1 for a step trajectory with finite jerk, could look like according to Eq. (3.10) and Figure 3.7

$$j_{fjerk1}(t) = \text{sign}(p_f) \cdot \begin{cases} j_{max} & \text{if } t_j > t \\ -j_{max} & \text{if } 3t_j > t \geq t_j \\ j_{max} & \text{if } 4t_j > t \geq 3t_j \\ 0 & \text{if } t \geq 4t_a \end{cases}, \tag{3.10}$$

where t_j [s] was the time with constant jerk (different from zero). The time t_j was unknown at this point, so an expression for this needed to be derived using p_f and j_{max}. This could be done through further integration.

The acceleration profile a_{fjerk1} was received by integration of j_{fjerk1}. Doing so resulted in a_{fjerk1} being according to Figure 3.8 and Eq. (3.11)

$$a_{fjerk1}(t) = \text{sign}(p_f) j_{max} \cdot \begin{cases} t & \text{if } t_j > t \\ 2t_j - t & \text{if } 3t_j > t \geq t_j \\ t - 4t_j & \text{if } 4t_j > t \geq 3t_j \\ 0 & \text{if } t \geq 4t_a \end{cases}. \tag{3.11}$$

The velocity profile v_{fjerk1} was received by integration of a_{fjerk1}. Doing so resulted in v_{fjerk1} being according to Figure 3.9 and Eq. (3.12)

$$v_{fjerk1}(t) = \text{sign}(p_f) j_{max} \cdot \begin{cases} \frac{t^2}{2} & \text{if } t_j > t \\ -\frac{t^2}{2} + 2t_j t - t_j^2 & \text{if } 3t_j > t \geq t_j \\ \frac{t^2}{2} - 4t_j t + 8t_j^2 & \text{if } 4t_j > t \geq 3t_j \\ 0 & \text{if } t \geq 4t_a \end{cases}. \tag{3.12}$$

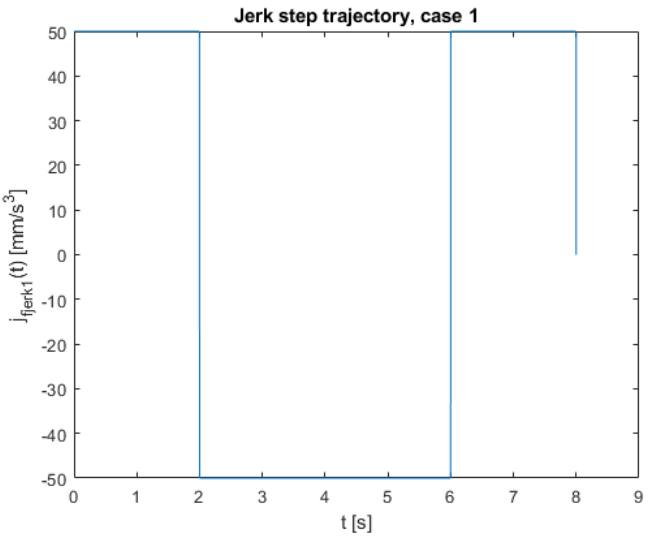

Figure 3.7 Plot of jerk step trajectory, Case 1, where $j_{max} = 50$ mm/s^3, $t_j = 2$ s and an assumption that $p_f > 0$.

The position profile p_{fjerk1} was received by integration of v_{fjerk1}. Doing so resulted in p_{fjerk1} being according to Figure 3.10 and Eq. (3.13)

$$p_{fjerk1}(t) = \text{sign}(p_f) j_{max} \cdot \begin{cases} \frac{t^3}{6} & \text{if } t_j > t \\ -\frac{t^3}{6} + t^2 t_j - t t_j^2 + \frac{t_j^3}{3} & \text{if } 3t_j > t \geq t_j \\ \frac{t^3}{6} - 2t_j t^2 + 8t_j^2 t - \frac{26t_j^3}{3} & \text{if } 4t_j > t \geq 3t_j \\ 2t_j^3 & \text{if } t \geq 4t_a \end{cases}. \quad (3.13)$$

Since p_f and j_{max} were given by the user, then t_j could be solved for using Eq. (3.13) when $t \geq 4t_a$. Doing so resulted in Eq. (3.14)

$$t_j = \sqrt[3]{\frac{|p_f|}{2j_{max}}}. \quad (3.14)$$

Case 2: Saturated velocity, unsaturated acceleration

If it was instead assumed that the velocity became saturated according to the desired maximum absolute velocity v_{max}, then a jerk trajectory $j_{fjerk2}(t)$ for a step trajectory, could look like according to Eq. (3.15) and Figure 3.11

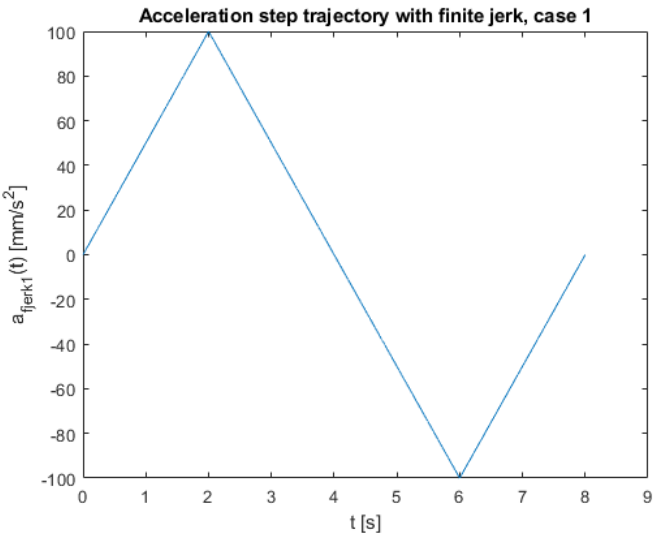

Figure 3.8 Plot of acceleration step trajectory with finite jerk, Case 1, where $j_{max} = 50$ mm/s^3, $t_j = 2$ s and an assumption that $p_f > 0$.

$$j_{fjerk2}(t) = \text{sign}(p_f) \cdot \begin{cases} j_{max} & \text{if } t_j > t \\ -j_{max} & \text{if } 2t_j > t \geq t_j \\ 0 & \text{if } t_v + 2t_j > t \geq 2t_j \\ -j_{max} & \text{if } t_v + 3t_j > t \geq t_v + 2t_j \\ j_{max} & \text{if } t_v + 4t_j > t \geq t_v + 3t_j \\ 0 & \text{if } t \geq t_v + 4t_j \end{cases}. \tag{3.15}$$

An expression for t_j and t_v needed to be derived using p_f, j_{max} and v_{max}. This could be done through further integration.

The acceleration profile a_{fjerk2} was received by integration of j_{fjerk2}. Doing so resulted in a_{fjerk2} being according to Figure 3.12 and Eq. (3.16)

$$a_{fjerk2}(t) = \text{sign}(p_f) j_{max} \cdot \begin{cases} t & \text{if } t_j > t \\ 2t_j - t & \text{if } 2t_j > t \geq t_j \\ 0 & \text{if } t_v + 2t_j > t \geq 2t_j \\ t_v + 2t_j - t & \text{if } t_v + 3t_j > t \geq t_v + 2t_j \\ t - t_v - 4t_j & \text{if } t_v + 4t_j > t \geq t_v + 3t_j \\ 0 & \text{if } t \geq t_v + 4t_j, \end{cases}. \tag{3.16}$$

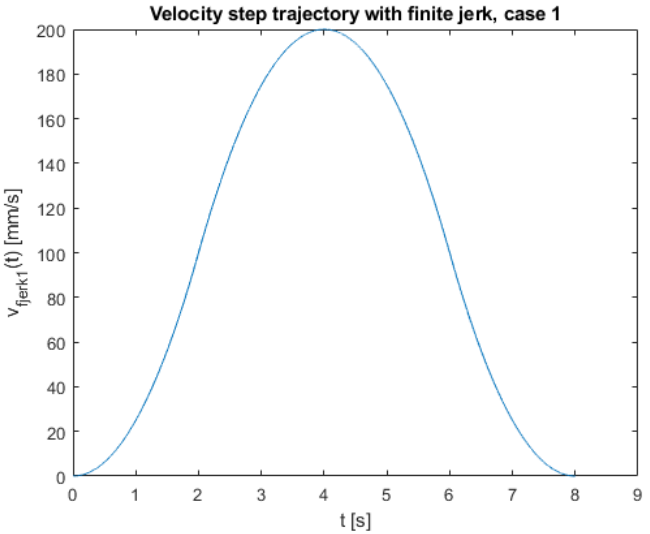

Figure 3.9 Plot of velocity step trajectory with finite jerk, Case 1, where $j_{max} = 50$ mm/s^3, $t_j = 2$ s and an assumption that $p_f > 0$.

where the maximum acceleration for the trajectory could be found at time $t = t_j$ (and minimum at time $t = t_a + 3t_j$). The maximum acceleration for the trajectory $a_{max/fjerk2}$ was given by Eq. (3.17)

$$a_{max/fjerk2} = j_{max} t_j. \tag{3.17}$$

The velocity profile v_{fjerk2} was received by integration of a_{fjerk2}. Doing so resulted in v_{fjerk2} being according to Figure 3.13 and Eq. (3.18)

$$v_{fjerk2}(t) = \text{sign}(p_f) j_{max} \cdot \tag{3.18}$$
$$\begin{cases} \frac{t^2}{2} & \text{if } t_j > t \\ -\frac{t^2}{2} + 2t_j t - t_j^2 & \text{if } 2t_j > t \geq t_j \\ t_j^2 & \text{if } t_v + 2t_j > t \geq 2t_j \\ -\frac{t^2}{2} + t(t_v + 2t_j) - \frac{t_v^2}{2} - 2t_v t_j - t_j^2 & \text{if } t_v + 3t_j > t \geq t_v + 2t_j \\ \frac{t^2}{2} - t(t_v + 4t_j) + 8t_j^2 + \frac{t_v^2}{2} + 4t_j t_v & \text{if } t_v + 4t_j > t \geq t_v + 3t_j \\ 0 & \text{if } t \geq t_v + 4t_j \end{cases}.$$

The position profile p_{fjerk2} was received by integration of v_{fjerk2}. Doing so resulted in p_{fjerk2} being according to Figure 3.14 and Eq. (3.19)

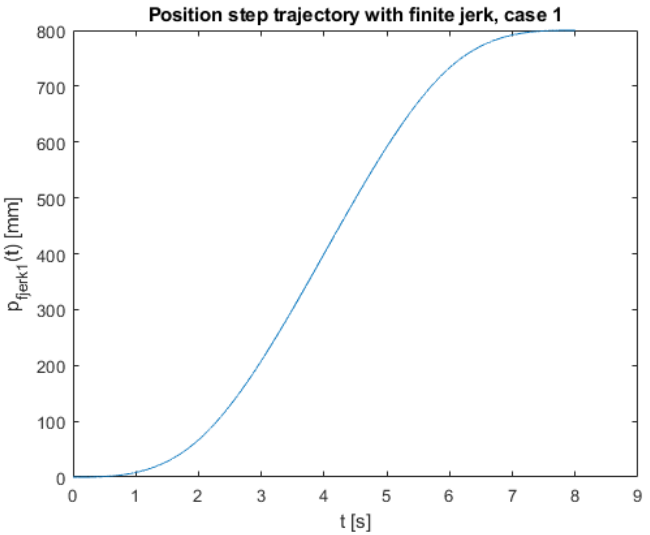

Figure 3.10 Plot of position step trajectory with finite jerk, Case 1, where $j_{max} = 50$ mm/s^3, $t_j = 2$ s and an assumption that $p_f > 0$..

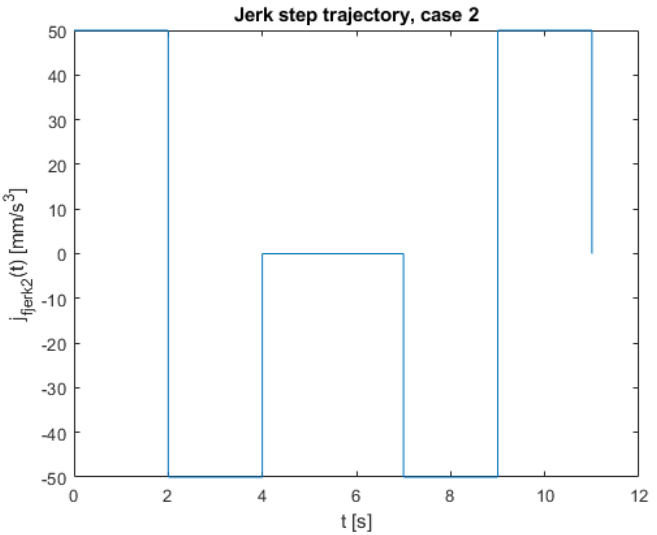

Figure 3.11 Plot of jerk step trajectory, Case 2, where $j_{max} = 50$ mm/s^3, $t_j = 2$ s, $t_v = 3$ s and an assumption that $p_f > 0$.

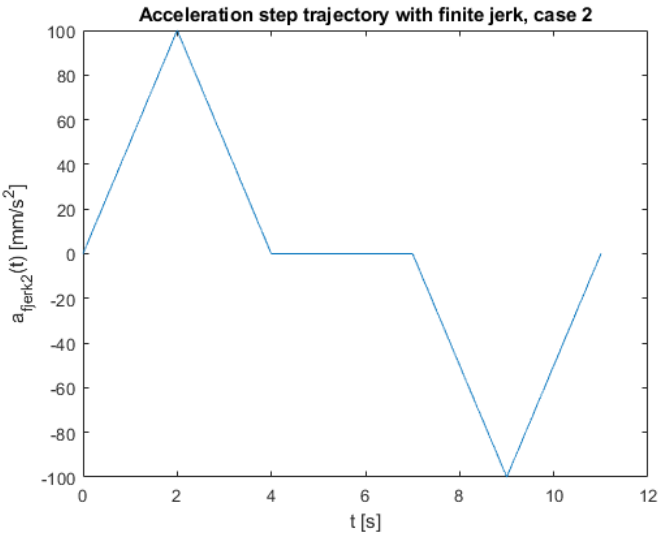

Figure 3.12 Plot of acceleration step trajectory with finite jerk, Case 2, where $j_{max} = 50$ mm/s^3, $t_j = 2$ s, $t_v = 3$ s and an assumption that $p_f > 0$.

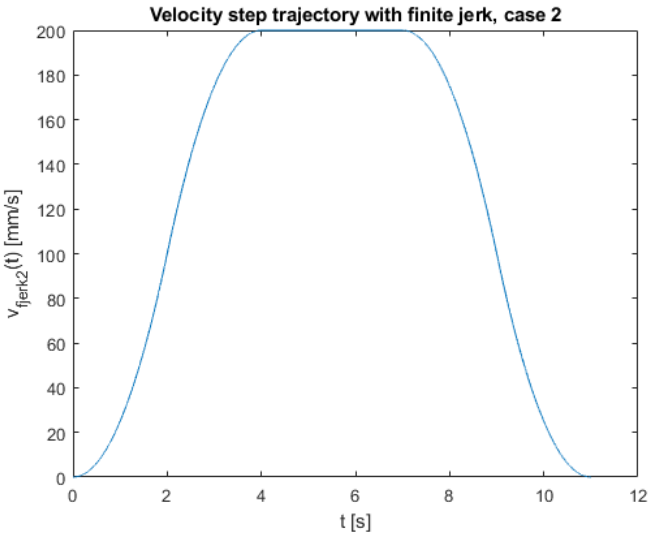

Figure 3.13 Plot of velocity step trajectory with finite jerk, Case 2, where $j_{max} = 50$ mm/s^3, $t_j = 2$ s, $t_v = 3$ s and an assumption that $p_f > 0$. This resulted in the maximum velocity being $v_{max} = 200$ mm/s.

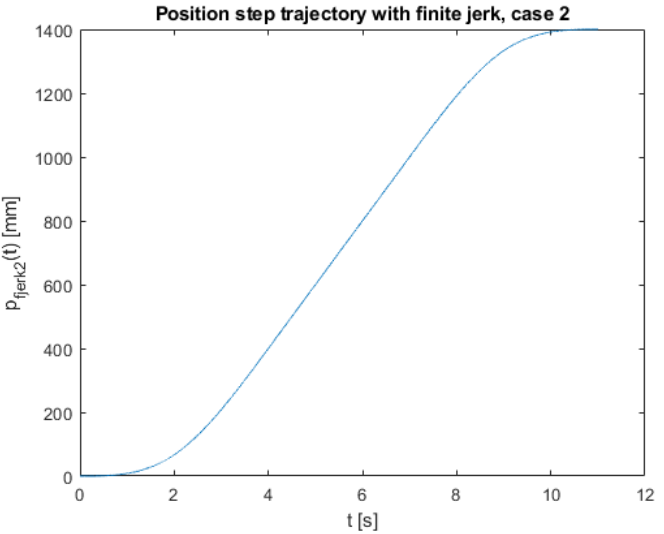

Figure 3.14 Plot of position step trajectory with finite jerk, Case 2, where $j_{max} = 50$ mm/s^3, $t_j = 2$ s, $t_v = 3$ s and an assumption that $p_f > 0$.

$$p_{fjerk2}(t) = \text{sign}(p_f) j_{max}. \tag{3.19}$$

$$\begin{cases} \frac{t^3}{6}, & \text{if } t_j > t \\ -\frac{t^3}{6} + t^2 t_j - t t_j^2 + \frac{t_j^3}{3}, & \text{if } 2t_j > t \geq t_j \\ t_j^2(t - t_j), & \text{if } t_v + 2t_j > t \geq 2t_j \\ \frac{1}{6}(-t^3 + t^2(6t_j + 3t_v) & \\ -t(6t_j^2 + 12t_j t_v + 3t_v^2) & \\ +2t_j^3 + 12t_j^2 t_v + 6t_j t_v^2 + t_v^3), & \text{if } t_v + 3t_j > t \geq t_v + 2t_j \\ -\frac{1}{6}(-t^3 + t^2(12t_j + 3t_v) & \\ -t(48t_j^2 + 24t_j t_v + 3t_v^2) & \\ +52t_j^3 + 42t_j^2 t_v + 12t_j t_v^2 + t_v^3), & \text{if } t_v + 4t_j > t \geq t_v + 3t_j \\ t_j^2(2t_j + t_v), & \text{if } t \geq t_v + 4t_j \end{cases}.$$

Since p_f, j_{max} and v_{max} were given by the user, and that the velocity saturated at v_{max}, then t_j and t_v could be solved for. t_j and t_v could be solved for by using Eq. (3.19) when $t \geq t_v + 4t_j$ and Eq. (3.18) when $t_v + 2t_j > t \geq 2t_j$. Doing so resulted in Eqs. (3.20) and (3.21)

$$t_j = \sqrt{\frac{v_{max}}{j_{max}}}, \tag{3.20}$$

$$t_v = \frac{|p_f|}{v_{max}} - 2\sqrt{\frac{v_{max}}{j_{max}}}. \tag{3.21}$$

Case 3: Unsaturated velocity, saturated acceleration

If it was instead assumed that the acceleration became saturated according to the desired maximum absolute velocity a_{max}, then a jerk trajectory $j_{fjerk3}(t)$ for a step trajectory, could look like according to Eq. (3.22) and Figure 3.15

$$j_{fjerk3}(t) = \text{sign}(p_f) \cdot \begin{cases} j_{max} & \text{if } t_j > t \\ 0 & \text{if } t_a + t_j > t \geq t_j \\ -j_{max} & \text{if } t_a + 3t_j > t \geq t_a + t_j \\ 0 & \text{if } 2t_a + 3t_j > t \geq t_a + 3t_j \\ j_{max} & \text{if } 2t_a + 4t_j > t \geq 2t_a + 3t_j \\ 0 & \text{if } t \geq 2t_a + 4t_j \end{cases}. \tag{3.22}$$

An expression for t_j and t_a needed to be derived using p_f, j_{max} and a_{max}. This could be done through further integration.

The acceleration profile a_{fjerk3} was received by integration of j_{fjerk3}. Doing so resulted in a_{fjerk3} being according to Figure 3.16 and Eq. (3.23)

$$a_{fjerk3}(t) = \text{sign}(p_f) j_{max} \cdot \begin{cases} t & \text{if } t_j > t \\ t_j & \text{if } t_a + t_j > t \geq t_j \\ 2t_j + t_a - t & \text{if } t_a + 3t_j > t \geq t_a + t_j \\ -t_j & \text{if } 2t_a + 3t_j > t \geq t_a + 3t_j \\ t - 4t_j - 2t_a & \text{if } 2t_a + 4t_j > t \geq 2t_a + 3t_j \\ 0 & \text{if } t \geq 2t_a + 4t_j \end{cases}. \tag{3.23}$$

The velocity profile v_{fjerk3} was received by integration of a_{fjerk3}. Doing so resulted in v_{fjerk3} being according to Figure 3.17 and Eq. (3.24)

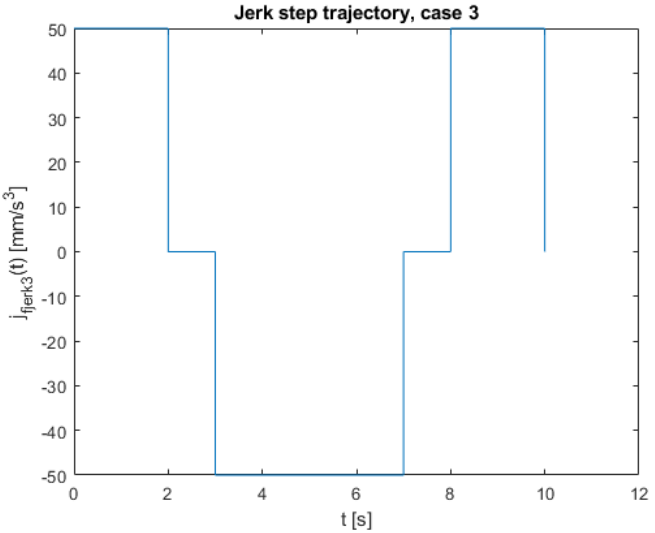

Figure 3.15 Plot of jerk step trajectory, Case 3, where $j_{max} = 50$ mm/s^3, $t_j = 2$ s, $t_a = 1$ s and an assumption that $p_f > 0$.

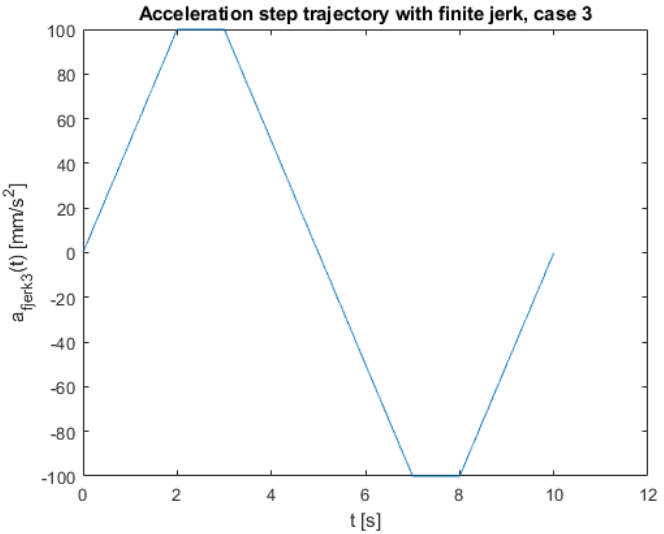

Figure 3.16 Plot of acceleration step trajectory with finite jerk, Case 3, where $j_{max} = 50$ mm/s^3, $t_j = 2$ s, $t_a = 1$ s and an assumption that $p_f > 0$. This resulted in the maximum acceleration being $a_{max} = 100$ mm/s^2.

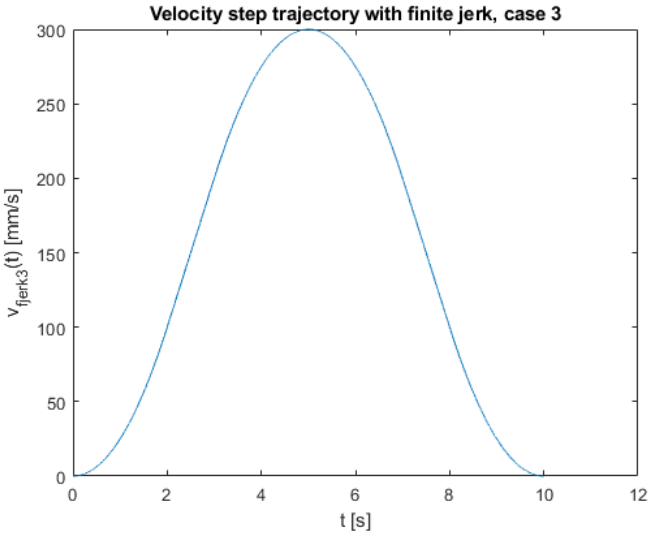

Figure 3.17 Plot of velocity step trajectory with finite jerk, Case 3, where $j_{max} = 50$ mm/s^3, $t_j = 2$ s, $t_a = 1$ s and an assumption that $p_f > 0$.

$$v_{fjerk3}(t) = \text{sign}(p_f) j_{max}. \tag{3.24}$$

$$\begin{cases} \frac{t^2}{2} & \text{if } t_j > t \\ t_j(t - \frac{t_j}{2}) & \text{if } t_a + t_j > t \geq t_j \\ \frac{1}{2}(-t^2 + t(2t_a + 4t_j) - t_a^2 - 2t_a t_j - 2t_j^2) & \text{if } t_a + 3t_j > t \geq t_a + t_j \\ \frac{t_j}{2}(4t_a - 2t + 7t_j) & \text{if } 2t_a + 3t_j > t \geq t_a + 3t_j \\ \frac{1}{2}(t^2 - t(4t_a + 8t_j) + 4t_a^2 + 16t_a t_j + 16t_j^2) & \text{if } 2t_a + 4t_j > t \geq 2t_a + 3t_j \\ 0 & \text{if } t \geq 2t_a + 4t_j \end{cases},$$

where the maximum velocity for the trajectory could be found at time $t = t_a + 2t_j$. The maximum velocity for the trajectory $v_{max/fjerk3}$ was given by Eq. (3.25)

$$v_{max/fjerk3} = j_{max} t_j (t_a + t_j). \tag{3.25}$$

The position profile p_{fjerk3} was received by integration of v_{fjerk3}. Doing so resulted in p_{fjerk3} being according to Figure 3.18 and Eq. (3.26)

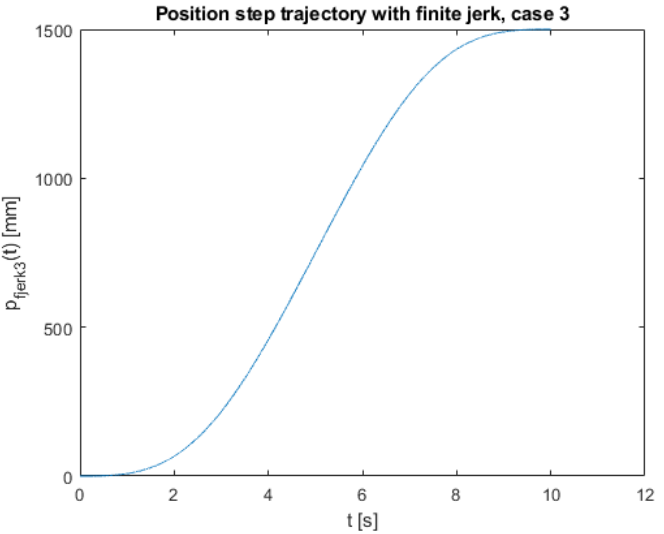

Figure 3.18 Plot of position step trajectory with finite jerk, Case 3, where $j_{max} = 50$ mm/s^3, $t_j = 2$ s, $t_a = 1$ s and an assumption that $p_f > 0$.

$$p_{fjerk3}(t) = \text{sign}(p_f) j_{max}. \tag{3.26}$$

$$\begin{cases} \frac{t^3}{6}, & \text{if } t_j > t \\ t_j(\frac{t^2}{2} - \frac{t_j t}{2} + \frac{t_j^2}{6}), & \text{if } t_a + t_j > t \geq t_j \\ \frac{1}{6}(-t^3 + t^2(3t_a + 6t_j) & \\ -t(3t_a^2 + 6t_a t_j + 6t_j^2) & \\ +t_a^3 + 3t_a^2 t_j + 3t_a t_j^2 + 2t_j^3), & \text{if } t_a + 3t_j > t \geq t_a + t_j \\ -\frac{t_j}{6}(3t^2 - t(12t_a + 21t_j) & \\ +6t_a^2 + 24t_a t_j + 25t_j^2), & \text{if } 2t_v + 3t_j > t \geq t_v + 3t_j \\ -\frac{1}{6}(-t^3 + t^2(6t_a + 12t_j) & \\ -t(12t_a^2 + 48t_a t_j + 48t_j^2) & \\ +8t_a^3 + 42t_a^2 t_j + 78t_a t_j^2 + 52t_j^3), & \text{if } 2t_v + 4t_j > t \geq 2t_v + 3t_j \\ t_j(t_a^2 + 3t_a t_j + 2t_j^2), & \text{if } t \geq 2t_v + 4t_j \end{cases}.$$

Since p_f, j_{max} and a_{max} were given by the user, and that the acceleration saturated at a_{max}, then t_j and t_a could be solved for. The times t_j and t_a could be solved for by using Eq. (3.26) when $t \geq 2t_v + 4t_j$ and Eq. (3.23) when $t_a + t_j > t \geq t_j$. Doing so resulted in Eqs. (3.27) and (3.28)

$$t_j = \frac{a_{max}}{j_{max}}, \tag{3.27}$$

$$t_a = -\frac{3a_{max}}{2j_{max}} + \sqrt{\frac{a_{max}^2}{4j_{max}^2} + \frac{|p_f|}{a_{max}}}. \tag{3.28}$$

Case 4: Saturated velocity, saturated acceleration

If it was assumed that both the acceleration and velocity became saturated according to a_{max} and v_{max}, then a jerk trajectory $j_{fjerk4}(t)$ for a step trajectory, could look like according to Eq. (3.29) and Figure 3.19

$$j_{fjerk4}(t) = \text{sign}(p_f) \cdot \begin{cases} j_{max} & \text{if } t_j > t \\ 0 & \text{if } t_a + t_j > t \geq t_j \\ -j_{max} & \text{if } t_a + 2t_j > t \geq t_a + t_j \\ 0 & \text{if } t_v + t_a + 2t_j > t \geq t_a + 2t_j \\ -j_{max} & \text{if } t_v + t_a + 3t_j > t \geq t_v + t_a + 2t_j \\ 0 & \text{if } t_v + 2t_a + 3t_j > t \geq t_v + t_a + 3t_j \\ j_{max} & \text{if } t_v + 2t_a + 4t_j > t \geq t_v + 2t_a + 3t_j \\ 0 & \text{if } t \geq t_v + 2t_a + 4t_j \end{cases}. \tag{3.29}$$

An expression for t_j, t_a and t_v needed to be derived using p_f, j_{max}, a_{max} and v_{max}. This could be done through further integration.

The acceleration profile a_{fjerk4} was received by integration of j_{fjerk4}. Doing so resulted in a_{fjerk4} being according to Figure 3.20 and Eq. (3.30)

$$a_{fjerk4}(t) = \text{sign}(p_f) j_{max} \cdot \tag{3.30}$$
$$\begin{cases} t & \text{if } t_j > t \\ t_j & \text{if } t_a + t_j > t \geq t_j \\ 2t_j + t_a - t & \text{if } t_a + 2t_j > t \geq t_a + t_j \\ 0 & \text{if } t_v + t_a + 2t_j > t \geq t_a + 2t_j \\ t_v + t_a + 2t_j - t & \text{if } t_v + t_a + 3t_j > t \geq t_v + t_a + 2t_j \\ -t_j & \text{if } t_v + 2t_a + 3t_j > t \geq t_v + t_a + 3t_j \\ t - (t_v + 2t_a + 4t_j) & \text{if } t_v + 2t_a + 4t_j > t \geq t_v + 2t_a + 3t_j \\ 0 & \text{if } t \geq t_v + 2t_a + 4t_j \end{cases}.$$

The velocity profile v_{fjerk4} was received by integration of a_{fjerk4}. Doing so resulted in v_{fjerk4} being according to Figure 3.21 and Eq. (3.31)

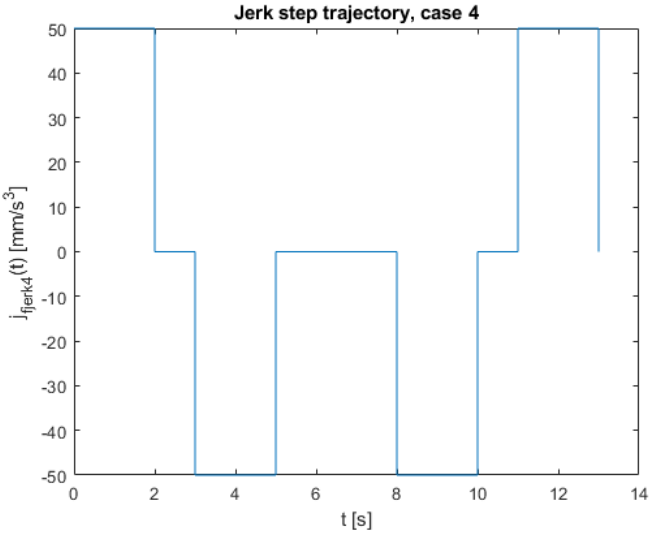

Figure 3.19 Plot of jerk step trajectory, Case 4, where $j_{max} = 50$ mm/s^3, $t_j = 2$ s, $t_a = 1$ s, $t_v = 3$ s and an assumption that $p_f > 0$.

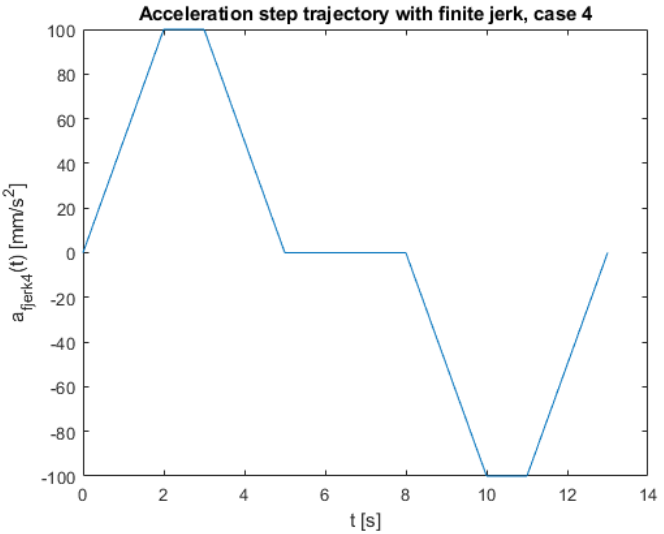

Figure 3.20 Plot of acceleration step trajectory with finite jerk, Case 4, where $j_{max} = 50$ mm/s^3, $t_j = 2$ s, $t_a = 1$ s, $t_v = 3$ s and an assumption that $p_f > 0$. This resulted in the maximum acceleration being $a_{max} = 100$ mm/s^2.

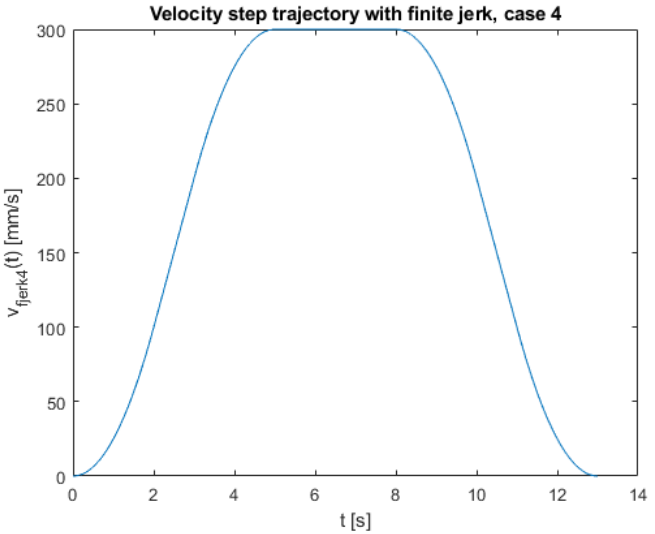

Figure 3.21 Plot of velocity step trajectory with finite jerk, Case 4, where $j_{max} = 50$ mm/s^3, $t_j = 2$ s, $t_a = 1$ s, $t_v = 3$ s and an assumption that $p_f > 0$. This resulted in the maximum velocity being $v_{max} = 300$ mm/s.

$$v_{fjerk4}(t) = \text{sign}(p_f) j_{max} \cdot \tag{3.31}$$

$$\begin{cases} \frac{t^2}{2}, & \text{if } t_j > t \\ t_j(t - \frac{t_j}{2}), & \text{if } t_a + t_j > t \geq t_j \\ -\frac{1}{2}(t^2 - t(2t_a + 4t_j) & \\ +t_a^2 + 2t_a t_j + 2t_j^2), & \text{if } t_a + 2t_j > t \geq t_a + t_j \\ t_j(t_a + t_j), & \text{if } t_v + t_a + 2t_j > t \geq t_a + 2t_j \\ -\frac{t^2}{2} + t(t_a + 2t_j + t_v) + t_j(t_a + t_j) & \\ -\frac{1}{2}(t_a + 2t_j + t_v)^2, & \text{if } t_v + t_a + 3t_j > t \geq t_v + t_a + 2t_j \\ \frac{t_j}{2}(-2t + 4t_a + 7t_j + 2t_v), & \text{if } t_v + 2t_a + 3t_j > t \geq t_v + t_a + 3t_j \\ \frac{1}{2}(-t + 2t_a + 4t_j + t_v)^2, & \text{if } t_v + 2t_a + 4t_j > t \geq t_v + 2t_a + 3t_j \\ 0, & \text{if } t \geq t_v + 2t_a + 4t_j \end{cases}.$$

The position profile p_{fjerk4} was received by integration of v_{fjerk4}. Doing so resulted in p_{fjerk4} being according to Figure 3.22 and Eq. (3.32)

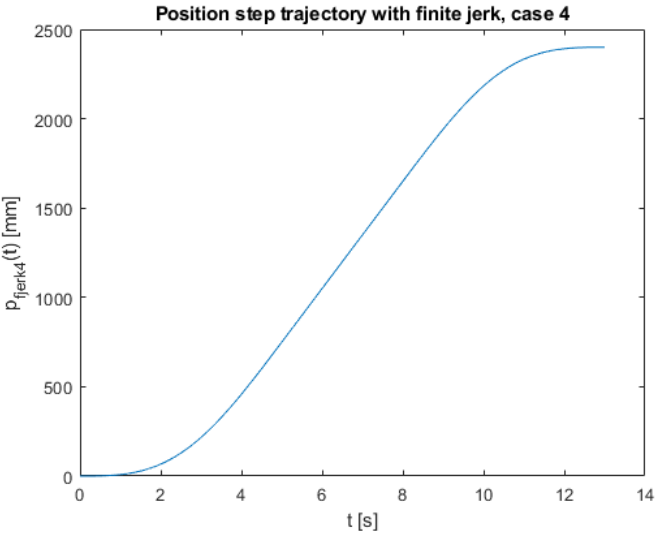

Figure 3.22 Plot of position step trajectory with finite jerk, Case 4, where $j_{max} = 50$ mm/s^3, $t_j = 2$ s, $t_a = 1$ s, $t_v = 3$ s and an assumption that $p_f > 0$.

$$p_{fjerk4}(t) = \text{sign}(p_f) j_{max}. \tag{3.32}$$

$$\begin{cases} \frac{t^3}{6}, \text{ if } t_j > t \\ t_j(\frac{t^2}{2} - \frac{t_j t}{2} + \frac{t_j^2}{6}), \text{if } t_a + t_j > t \geq t_j \\ \frac{1}{6}(-t^3 + t^2(3t_a + 6t_j) - t(3t_a^2 + 6t_a t_j + 6t_j^2) + t_a^3 + 3t_a^2 t_j + 3t_a t_j^2 + 2t_j^3), \\ \text{if } t_a + 2t_j > t \geq t_a + t_j \\ -\frac{t_j}{2}(t_a + t_j)(t_a - 2t + 2t_j), \text{if } t_v + t_a + 2t_j > t \geq t_a + 2t_j \\ \frac{1}{6}(-t^3 + t^2(3t_a + 6t_j + 3t_v) - t(3t_a^2 + 6t_a t_j + 6t_a t_v + 6t_j^2 + 12t_j t_v + 3t_v^2) \\ +t_a^3 + 3t_a^2 t_j + 3t_a^2 t_v + 3t_a t_j^2 + 12t_a t_j t_v + 3t_a t_v^2 + 2t_j^3 + 12t_j^2 t_v + 6t_j t_v^2 + t_v^3), \\ \text{if } t_v + t_a + 3t_j > t \geq t_v + t_a + 2t_j \\ -\frac{t_j}{6}(3t^2 - t(12t_a + 21t_j + 6t_v) + 6t_a^2 + 24t_a t_j + 6t_a t_v + 25t_j^2 + 15t_j t_v + 3t_v^2), \\ \text{if } t_v + 2t_a + 3t_j > t \geq t_v + t_a + 3t_j \\ \frac{1}{6}(-(2t_a - t + 4t_j + t_v)^3 + t_j(6t_a^2 + 18t_a t_j + 6t_v t_a + 12t_j^2 + 6t_v t_j)), \\ \text{if } t_v + 2t_a + 4t_j > t \geq t_v + 2t_a + 3t_j \\ t_j(t_a + t_j)(t_a + 2t_j + t_v), \text{ if } t \geq t_v + 2t_a + 4t_j \end{cases}.$$

Since p_f, j_{max}, a_{max} and v_{max} were given by the user, and that both the acceleration and velocity saturated, then t_j, t_a and t_v could be solved for. The times t_j, t_a and

t_v could be solved for by using Eq. (3.32) when $t \geq t_v + 2t_a + 4t_j$, Eq. (3.30) when $t_a + t_j > t \geq t_j$ and Eq. (3.31) when $t_v + t_a + 2t_j > t \geq t_a + 2t_j$. Doing so resulted in Eqs. (3.33), (3.34) and (3.35)

$$t_j = \frac{a_{max}}{j_{max}}, \tag{3.33}$$

$$t_a = \frac{j_{max} v_{max} - a_{max}^2}{j_{max} a_{max}}, \tag{3.34}$$

$$t_v = \frac{|p_f| a_{max} j_{max} - v_{max}^2 j_{max} - a_{max}^2 v_{max}}{a_{max} v_{max} j_{max}}. \tag{3.35}$$

Case selection

Given p_f, j_{max}, a_{max} and v_{max}, it was needed to know which case to select for the step trajectory. One strategy was to evaluate the sign for t_a and t_v, together with the maximum acceleration for Case 2 $a_{max/fjerk2}$ and the maximum velocity for Case 3 $v_{max/fjerk3}$. An example of how this could be done was as follows.

- Case 4: If $t_a \geq 0$ in Eq. (3.34) and $t_v \geq 0$ in Eq. (3.35)
- Case 3: If not Case 4, $t_a \geq 0$ in Eq. (3.28) and $v_{max/fjerk3} \leq v_{max}$ in Eq. (3.25)
- Case 2: If not Case 3, $t_v \geq 0$ in Eq. (3.21) and $a_{max/fjerk2} \leq a_{max}$ in Eq. (3.17)
- Case 1: Otherwise

Once again, when the case had been determined, then the acceleration, velocity and position trajectories to the corresponding case were initialised and used to control the cart.

3.2 Cosine trajectory

For a more dynamic trajectory compared to only taking a step, a cosine position trajectory was used. A position-, velocity- and acceleration trajectory was generated according to Eqs. (3.36), (3.37) and (3.38)

$$p_{cos}(t) = A_{cos}(1 - \cos\frac{2\pi}{T_{cos}}t), \tag{3.36}$$

$$v_{cos}(t) = A_{cos}\frac{2\pi}{T_{cos}}\sin\frac{2\pi}{T_{cos}}t, \tag{3.37}$$

$$a_{cos}(t) = A_{cos}\left(\frac{2\pi}{T_{cos}}\right)^2\cos\frac{2\pi}{T_{cos}}t, \tag{3.38}$$

where A_{cos} [mm] was the amplitude and T_{cos} [s] the period of the position cosine trajectory.

The trajectories p_{cos} and v_{cos} were chosen this way as it resulted in the initial position and velocity to be zero. If this would not be the case, then the cart would jerk each time the trajectory was started.

3.3 Stationary position point determination

For this master thesis, it was be important for the system to at any time know the next upcoming stationary position point. Because of this, whenever a trajectory was initialised, a new array s_{traj} was also initialised which contained the next upcoming stationary position point.

The array s_{traj} was initialised by iterating backwards through v_{traj}. Assume that at an index i there was $|v_{traj}(i)| < \delta_v$, where δ_v [mm/s] was a very small number. The stationary position point $p_{traj}(i)$ was then stored in s_{traj}. $p_{traj}(i)$ was stored in s_{traj} until $|v_{traj}(j)| < \delta_v$ at a new index j held, where the new value $p_{traj}(j)$ was then stored in s_{traj} instead. For the case where the trajectory was repeated, which was the case for the cosine trajectory, then this iteration was done once again until a stationary point in s_{traj} was reached.

For this master thesis, $\delta_v = 10^{-10}$ mm/s was chosen.

4

Control without backlash compensation

For control without backlash compensation, the control structure was as in Figure 4.1. In this section, both motors were used at all times and were fed the same torque reference. Furthermore, the entire system could be divided into subsystems according to the following sections.

Signals in Figure 4.1 meant as follows.

- p [mm]: Position relative to starting point
- p_{traj} [mm]: Position reference from trajectory
- p_{error} [mm]: Position error
- $p_{globtraj}$ [mm]: Global position reference from trajectory
- v [mm/s]: Velocity
- v_{ref} [mm/s]: Velocity reference from velocity regulator
- v_{traj} [mm/s]: Velocity reference from trajectory
- v_{totref} [mm/s]: Total velocity reference
- v_{error} [mm/s]: Velocity error
- a_{traj} [mm/s^2]: Acceleration from trajectory
- s_{traj} [mm]: Upcoming stationary position point in trajectory
- τ_{ref} [316.92 mNm]: Torque reference from regulator
- τ_{dyn} [316.92 mNm]: Torque reference from dynamic model
- τ_{fric} [316.92 mNm]: Torque reference from friction model
- τ_{ff} [316.92 mNm]: Torque reference from torque feed forward

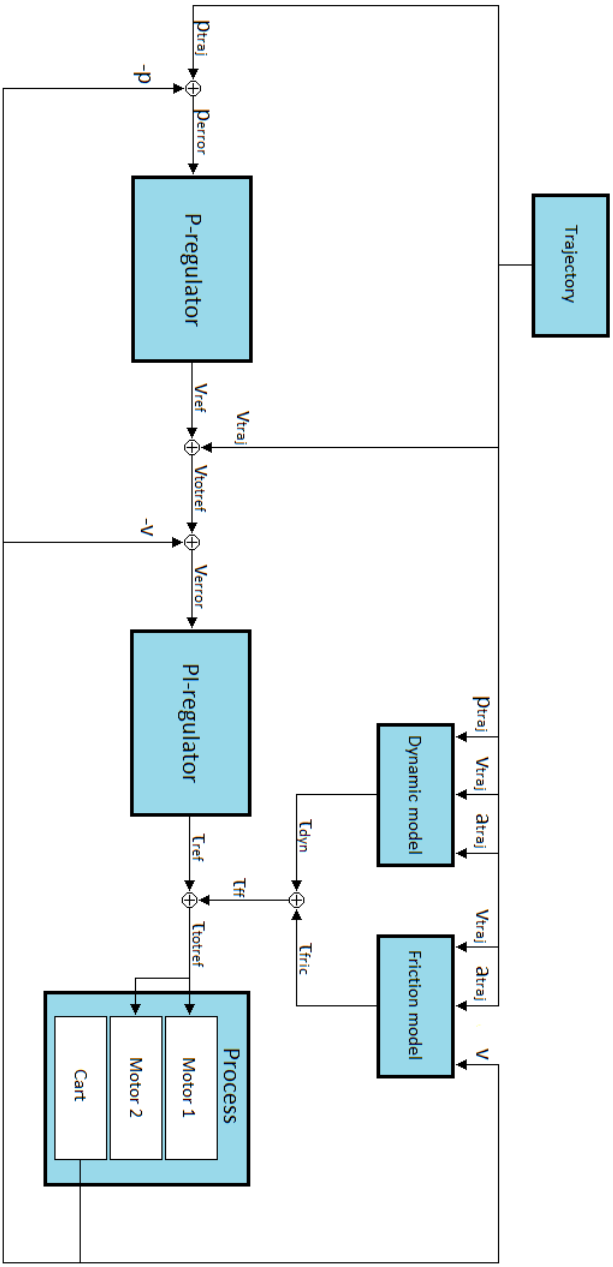

Figure 4.1 The control structure used without backlash compensation.

4.1 Velocity control

First, the unfiltered velocity $v_{uflt}(k)$ [mm/s] at sample time k was calculated using the cart position. This was done through a backwards approximation of the cart position derivative according to Eq. (4.1)

$$v_{uflt}(k) = \frac{p(k) - p(k-1)}{h}, \tag{4.1}$$

where p [mm] was the cart position relative to the starting point of the cart.

The unfiltered velocity $v_{uflt}(k)$ was filtered using a low-pass filter to remove high frequency noise. The filtered velocity $v_{flt}(k)$ [mm/s] was calculated according to Eq. (4.2)

$$v_{flt}(k) = v_{flt}(k-1)e^{-\omega_v h} + v_{uflt}(k)(1 - e^{-\omega_v h}), \tag{4.2}$$

where ω_v [rad/s] was the cutoff frequency.

As the joint can travel at high speeds of approximately 300 mm/s, and implemented robot joints are desired to go even faster, it was decided to have very little low-pass filtering as to avoid introducing delays in the velocity measurements. Choosing $\omega_v = 2000$ [rad/s] was deemed to be sufficient for this master thesis.

PI-control with anti-windup

The cart velocity could be controlled according to Eq. (4.3)

$$\tau_{ref}(t) = K_v(v_{totref}(t) - v_{flt}(t)) + K_{i/v}\int_0^t v_{totref}(x) - v_{flt}(x)dx, \tag{4.3}$$

where K_v and $K_{i/v}$ were the PI-parameters for velocity control. To avoid windup of the controller, then the integral part would not update if the control signal became saturated.

The tuning philosophy for velocity control was to increase K_v until noise in the control signal was deemed too big. Then, the value for $K_{i/v}$ was chosen slightly before signs of instability started to appear in the step responses, whilst also not resulting in a too large overshoot or too damped response for any velocity step responses. Using this tuning philosophy, then tuning parameters according to Table 4.1 were received.

Using this tuning however did not result in satisfactory velocity step responses across the entire velocity bandwidth. Velocity step responses using low velocity references resulted in overshoots.

PI-control with gain scheduling and anti-windup

To get desired velocity step responses across the entire velocity bandwidth, gain scheduling could be implemented. The cart was once again controlled according to Eq. (4.3), but using gain scheduling of the integral gain $K_{i/v}(|v_{totref}|)$ instead to

Table 4.1 Tuning for velocity control using a PI-regulator (with anti-windup).

Parameter	Value
K_v	37.5
$K_{i/v}$	350

Table 4.2 Tuning for velocity control using gain scheduling without any compensation.

Parameter	Value
K_v	37.5
$K_{i/v}(\lvert v_{totref}\rvert)$	$0.575\lvert v_{totref}\rvert + 38.5$

try and reduce overshoots for lower velocities. The tuning philosophy was to find values for $K_{i/v}$ which resulted in no over/undershoot when evaluating velocity step responses. Two velocity references were chosen, where one was small and one is large. A linear equation $K_{i/v}(|v_{totref}|)$ was then determined between these two found values for $K_{i/v}$.

Tuning for velocity control using gain scheduling without any compensation could be summarised in Table 4.2. Using this control strategy resulted in satisfactory velocity step responses across the entire velocity bandwidth. However, this control strategy resulted in a very low integrator gain for low velocities.

PI-control with reference weight and anti-windup

To reduce overshoot, a reference weight for the proportional term could also be added instead [Hägglund, 2015, pg.111]. Equation (4.3) was modified to Eq. (4.4)

$$\tau_{ref}(t) = K_v(\beta_v v_{totref}(t) - v_{flt}(t)) + K_{i/v}\int_0^t v_{totref}(x) - v_{flt}(x)dx, \tag{4.4}$$

where $\beta_v \in [0,1]$ was the reference weight parameter.

The tuning philosophy here was to use tuning according to Table 4.1, and where β_v was decreased until overshoots for low velocities had disappeared. Tuning for velocity control using reference weight without any compensation could be summarised in Table 4.3. Using this approach resulted in good performance when evaluating velocity step responses across the entire velocity bandwidth.

However, using a reference weight in the velocity control introduced a significant delay when using velocity trajectories, as seen in Figure 4.2.

Table 4.3 Tuning for velocity control using reference weight without any compensation.

Parameter	Value
K_v	37.5
$K_{i/v}$	350
β_v	0.65

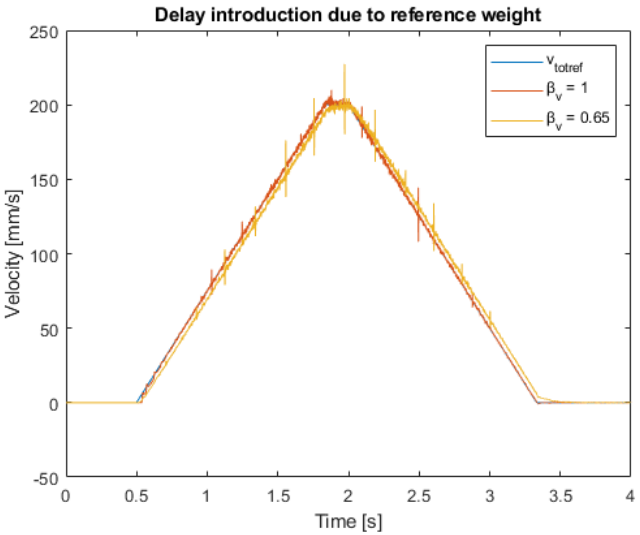

Figure 4.2 Using a reference weight for velocity control introduced a significant delay when following trajectories.

Velocity control conclusion

As mentioned before, gain scheduling resulted in a very low integral action for low velocities, despite good results when only evaluating velocity step responses. This made it so that control with disturbances would be compromised, making this alternative not suitable for desired applications of the robot.

Instead using a reference weight resulted in a significant delay being introduced when following trajectories, also despite good results when only evaluating velocity step responses. Due to this delay, position accuracy would greatly be compromised, also making this alternative not suitable.

Therefore, a simple PI-regulator with anti-windup was used for velocity control in this master thesis, as it seemed to have the least negative drawback of having overshoots for low velocities. This would hopefully not be as big of an issue, due to

the velocity references coming from a trajectory rather than as a step.

4.2 Position control

For position control, a P-regulator was used in cascade with the velocity control. Control was done according to Eq. (4.5)

$$v_{ref}(t) = K_p(p_{ref}(t) - p(t)). \tag{4.5}$$

The tuning philosophy for choosing K_p was to have it as large as possible without signs of oscillations due to instability when following trajectories. The resulting tuning without any compensation was summarised in Table 4.4.

Table 4.4 Tuning for position-velocity cascade control without any compensation.

Parameter	Value
K_v	37.5
$K_{i/v}$	350
K_p	60

4.3 Torque feed forward

To reduce work by the cascade-controlled regulators, torque could be fed forward to the process using known properties of the system. Two of these known properties was friction and the mechanical dynamics. Models for these two properties were derived below.

Friction model

Ideally there would be no friction, which would make it so that there would be no stationary motor torque required for the cart to maintain a constant velocity. Since this was not the case, then the stationary motor torque could be seen as a result of the viscous friction.

A friction model was derived by first measuring the stationary motor torque reference required to keep the cart at different velocities, and doing a piece-wise polynomial fit on the data. To avoid rapid switching of the friction model at low velocities, a separate function for the sign of the friction model was also derived. The friction model τ_{fric} was as in Eq. (4.6)

$$\tau_{fric} = \text{sign}_{fric} \cdot \text{mag}_{fric}, \tag{4.6}$$

where sign_{fric} was the function determining the sign of the friction model, and mag_{fric} determining the magnitude.

Magnitude of the friction model For the magnitude of the friction model, then a simplified model was derived which excluded temperature dependencies and effects of dynamic friction. The magnitude of the friction model was determined as the stationary motor torque for a velocity reference. The stationary motor torque was derived by heavy low-pass filtering of τ_{totref} similar to Eq. (4.2). The stationary motor torque was then measured as the filtered value of τ_{totref} when transients had disappeared from a velocity step response. The magnitude of the friction model $\text{mag}_{fric}(|v_{flt}|)$ was then defined as the piece-wise polynomial fit, where polynomials switched at their intersections. Data from the friction experiment together with the piece-wise polynomial fit could be seen in Figure 4.3.

Looking at Figure 4.3, it could be seen that polynomial 1 may be from Stribeck friction, and that polynomial 2 may be from viscous friction. The intersection of polynomial 1 and 2 may therefore contain information about the Coulomb friction.

Interesting dynamics seemed to appear for velocities over 200 mm/s. A near linear viscous friction was expected, but in figure 4.3, it could be seen that polynomials 3, 4 and 5 clearly violated this assumption. A reason for this may have been that an unknown dynamic in the system had larger gain for higher velocities. Polynomials 3, 4 and 5 were therefore discarded, and it was decided that the cart was not to be brought above 200 mm/s. Resulting magnitude of the friction model was seen in Figure 4.4 and Eq. (4.7)

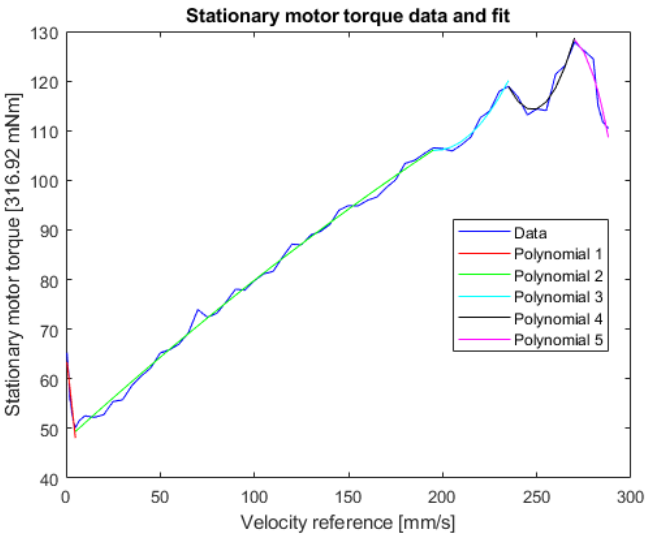

Figure 4.3 Plot of stationary motor torque reference versus velocity reference together with piece-wise polynomial fit. Interesting dynamics seemed to appear for velocities over 200 mm/s.

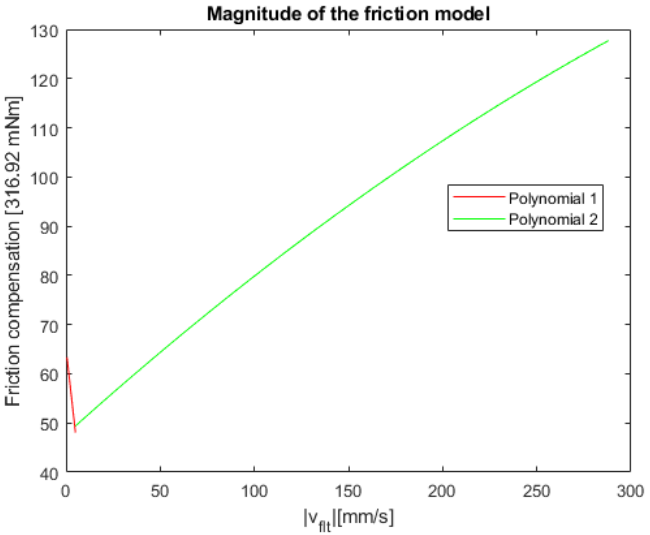

Figure 4.4 Resulting magnitude of the friction model. The cart was not to be brought above 200 mm/s.

The resulting model for the magnitude of the friction compensation could be seen in Eq. (4.7)

$$\text{mag}_{fric}(|v_{flt}|) = \begin{cases} -3.40|v_{flt}| + 65.1 & \text{if } |v_{flt}| < 4.65 \\ -0.000233|v_{flt}|^2 + 0.345|v_{flt}| + 47.7 & \text{if } 4.65 \leq |v_{flt}| \end{cases}. \quad (4.7)$$

It may be tempting to model static friction by using polynomial 1 only when the cart had remained stationary and started to accelerate, and then when the cart decelerated back to zero velocity, to use polynomial 2 to model dynamic friction. However it was not certain that polynomial 1 actually represented static friction, and that polynomial 2 actually represented dynamic friction. It was also difficult to measure dynamic friction for the cart for low velocities. Therefore mag_{fric} according to Figure 4.4 and Eq. (4.7) was used, where polynomial 1 was used at all times, despite if the cart accelerated from zero velocity or if the cart decelerated to zero velocity.

Sign of the friction model using s_{traj} To avoid rapid switching at zero velocity, special care needed to be taken for the sign of the friction model around this area. The position measurement p contained much less noise than v_{flt}, which made p very suitable for determination of the sign of the friction model. One way this could be done was by using knowledge of the next stopping point, given by s_{traj}. The sign

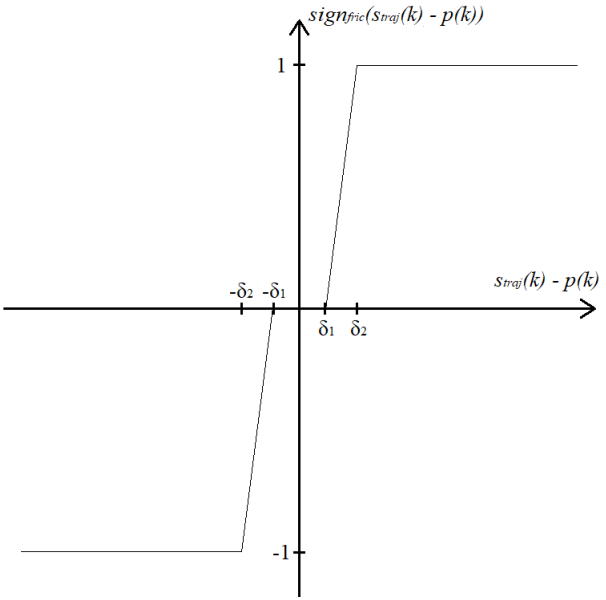

Figure 4.5 Sign for the friction model. δ_1 and δ_2 are manually chosen threshold values, where $0 \leq \delta_1 \leq \delta_2$.

of the friction using s_{traj}, $\text{sign}_{fric/s}$, could be defined according to Figure 4.5 and Eq. (4.8)

$$\text{sign}_{fric/s} = \begin{cases} 0 & |e_s(k)| < \delta_1 \\ \frac{1}{\delta_2 - \delta_1} e_s(k) - \frac{\delta_1}{\delta_2 - \delta_1} & \delta_1 \leq e_s(k) < \delta_2 \\ \frac{1}{\delta_2 - \delta_1} e_s(k) + \frac{\delta_1}{\delta_2 - \delta_1} & -\delta_1 \geq e_s(k) > -\delta_2 \\ 1 & \delta_2 \leq e_s(k) \\ -1 & -\delta_2 \geq e_s(k) \end{cases} . \tag{4.8}$$

where $e_s(k) = s_{traj}(k) - p(k)$ was the position error relative to the stationary position point.

Using $\text{sign}_{fric/s}$ would make it so that the friction model to some extent helped when external disturbances affected the cart. However, oscillatory behaviour could be introduced if δ_1 and δ_2 were not chosen with care.

Sign of the friction model using v_{traj} Another way to define the sign of the friction model was by using the velocity trajectory v_{traj}. This approach would not introduce any noise and would not risk adding any oscillatory behaviour, as the trajectory was predetermined. The function $\text{sign}_{fric/v}$ at sample time k could be defined according to Eq. (4.9)

$$\text{sign}_{fric/v} = \begin{cases} 1 & \text{if } v_{traj}(k) > \delta_v \\ -1 & \text{if } v_{traj}(k) < -\delta_v \\ \text{sign}_{fric/v}(v_{traj}(k-1)) & \text{if } |v_{traj}(k)| \leq \delta_v \\ 0 & \text{otherwise.} \end{cases} \tag{4.9}$$

where δ_v [mm/s] was a very small number.

Note that Eq. (4.9) did not say $\text{sign}_{fric}(v_{traj}(k)) = 0$, if $|v_{traj}(k)| < \delta_v$. The reason for this was that the cart will not have reached the desired destination as $|v_{traj}(k)| < \delta_v$ when $|v_{traj}(k-1)| \geq \delta_v$. Since very little position overshoot was desired, then the velocity of the cart should be in the same direction as it approached from, despite $|v_{traj}(k)| < \delta_v$, hence the sign of the friction model should be preserved in this case. If $|v_{traj}(0)| < \delta_v$, then the sign of the friction model was initialised to zero.

However, using $\text{sign}_{fric/v}$ did not make it so that the friction model helped when the cart was subjected to external disturbances. Using $\text{sign}_{fric/v}$ also made it so that the friction model was not true to some extent, as the friction model would be active despite after the cart having become stationary.

Friction model conclusion An evaluation was made using either $\text{sign}_{fric/s}$ or $\text{sign}_{fric/v}$. When using $\text{sign}_{fric/s}$ it was observed that large limit cycles would in certain situations be introduced if the cart was subjected to external disturbances. For this reason it was decided that $\text{sign}_{fric/s}$ was to be used in this master thesis.

Note that because additional torque was fed to the motor with a friction model, the tuning for the velocity PI-regulator was needed to be updated to compensate for the additional overshoot introduced to the velocity step responses. Tuning parameters for the cascade control using friction compensation are summarised in Table 4.5.

Table 4.5 Tuning for position-velocity cascade control with friction compensation.

Parameter	Value
K_v	37.5
$K_{i/v}$	275
K_p	60

Dynamic model

To control the cart, then an error needed to propagate through the cascade control seen in Figure 4.1. If a predicted torque would be fed to the motors, then the system would be faster as there would be no need to wait for this error to propagate.

One way the torque was able to be predicted was with classical mechanics. When trajectories were used to control the cart, then the desired position, velocity

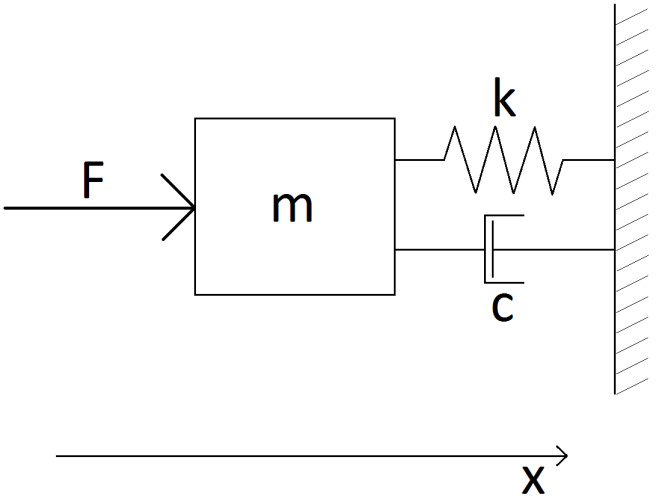

Figure 4.6 Classical mechanics analogy to Eq. (4.10), where F [N] was the force applied to the cart, m [kg] the mass of the cart, k [N/m] the spring constant, c [N/(m/s)] the damping constant and x [m] the position coordinate axis. Solving for F using Newton's second law resulted in $F = m\ddot{x} + c\dot{x} + kx$.

and acceleration were already known, which made it so that the torque to some extent was also already known.

A model for the torque was defined as Eq. (4.10)

$$\tau_{dyn} = b_1 p_{globtraj} + b_2 v_{traj} + b_3 a_{traj}, \tag{4.10}$$

where $b_1, b_2, b_3 \in \mathbb{R}$ and $p_{globtraj}$ [mm] is the global trajectory position. A classical mechanics analogy to Eq. (4.10) could be seen in Figure 4.6.

The parameters b_1, b_2 and b_3 could be identified by using a least squares method with known data about position, velocity, acceleration and torque.

Assume that data at n time instants have been gathered, and that position, velocity and acceleration data was given by the columns of an n-by-3 matrix X. Also assume that torque data was given by a n-by-1 column vector y. Then a 3-by-1 column vector $b = [b_1\ b_2\ b_3]^T$ could be solved for according to Eq. (4.11) [MathWorks, 2019a]

$$b = (X^T X)^{-1} X^T y. \tag{4.11}$$

Data was gathered by letting the cart follow trajectories, whilst storing the global position measurements p_{global} and the torque reference τ_{ref}. These position measurements were then differentiated and processed with low-pass and MA-filters to receive velocity and acceleration. The torque reference values were also processed

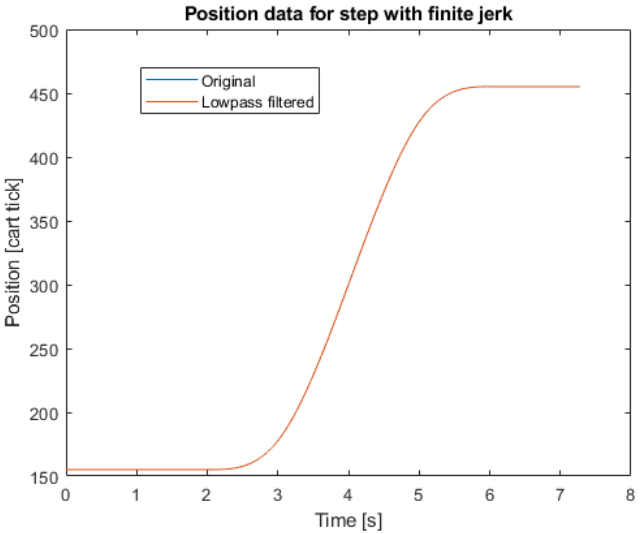

Figure 4.7 Position data from a step trajectory with finite jerk both with and without filtering.

with Hampel- (outlier removal), low-pass- and MA-filters. The data was processed offline in a non-causal manner, allowing for compensation of introduced delays.

In the following data gathering, tuning according to Table 4.5 was used. The friction model was active, and v_{traj} was also fed to the position P-regulator. Four trajectories were used to gather the data. The data was then treated using the Matlab functions *hampel*, *lowpass* and $filter$ described in [MathWorks, 2019b].

An example of data for a step trajectory with finite jerk is given in Figures 4.7, 4.8, 4.9 and 4.10.

The final position, velocity and acceleration data used to gather the coefficients b_1, b_2 and b_3 could be seen in Figure 4.11, and the final torque reference data together with the least squares fit could be seen in Figure 4.12. Using this data resulted in b_1, b_2 and b_3 being identified according to Eq. (4.12)

$$b = \begin{bmatrix} b_1 \\ b_2 \\ b_3 \end{bmatrix} = \begin{bmatrix} -0.00244 \\ -0.0120 \\ 0.493 \end{bmatrix} \tag{4.12}$$

Looking at Figure 4.12, then the torque estimate seemed to follow the data well. There were however two regions where the estimate did not seem to follow the data. These regions were for data after a trajectory step had been taken.

The reason for this mismatch may be because of the friction model, more specifically the sign of the friction model. This made it so that the regulators needed to

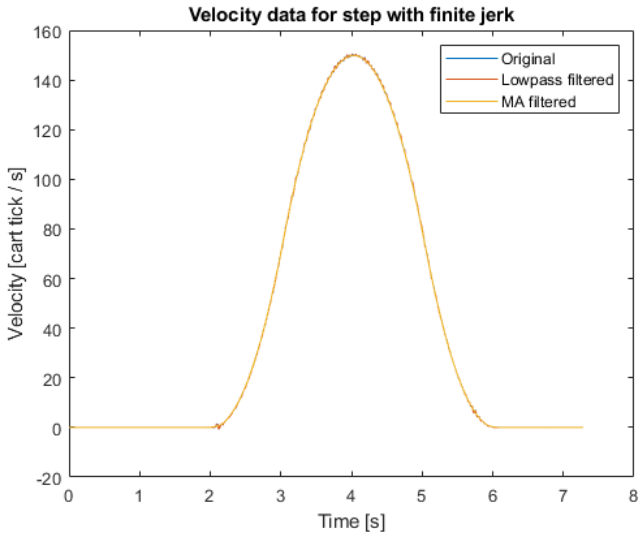

Figure 4.8 Velocity data from differentiation of processed data in Figure 4.7. This was then filtered using a low-pass filter followed by an MA-filter.

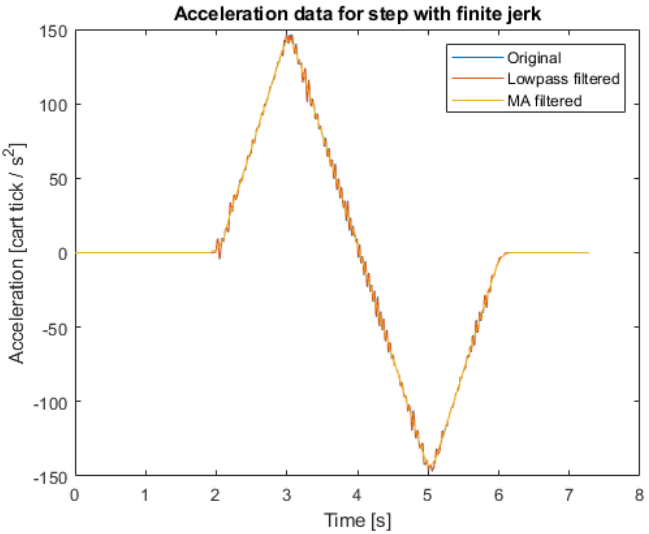

Figure 4.9 Acceleration data from differentiation of processed data in Figure 4.8. This was then filtered using a low-pass filter followed by an MA-filter.

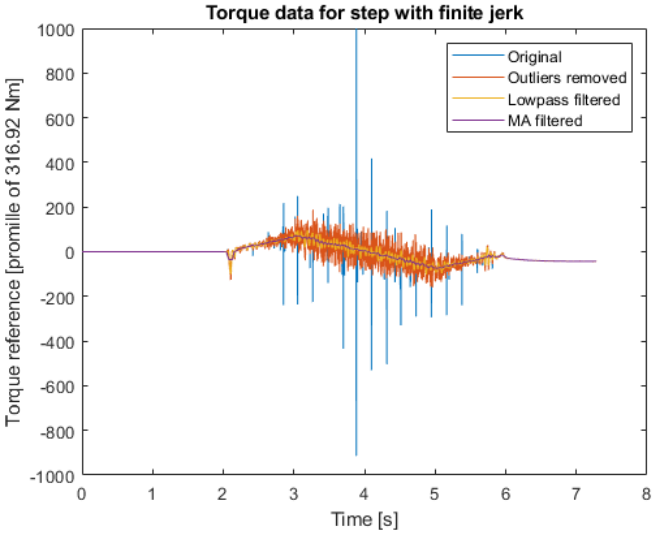

Figure 4.10 Torque reference data τ_{ref} from a step trajectory with finite jerk. This was then processed with a Hampel filter (outlier removal) followed by a low-pass filter and lastly an MA-filter.

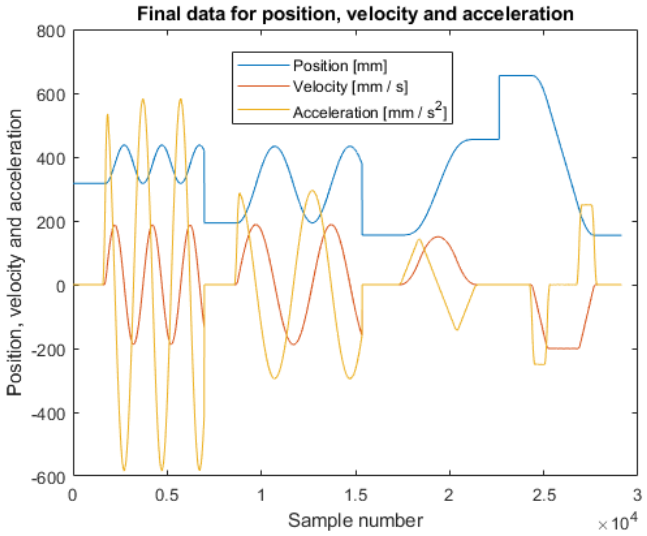

Figure 4.11 Final position, velocity and acceleration data used to identify coefficients b_1, b_2 and b_3.

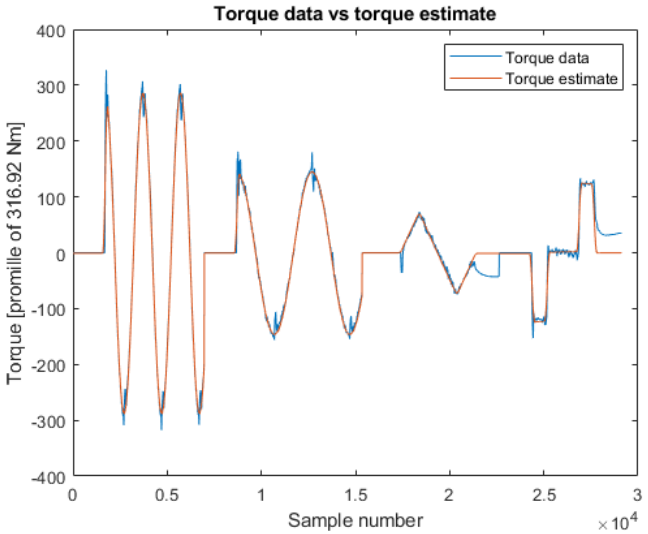

Figure 4.12 Final torque reference data used to gather coefficients b_1, b_2 and b_3, together with the least squares fit.

work at the endpoint of the step trajectories to compensate for the friction model being active. The estimate did not take this into account.

Looking at Figure 4.12, it could also be seen that the torque estimate did not seem follow data as the cart started moving in the beginning of each individual trajectory.

Conclusion of torque feed forward

With an ideal torque feed forward and no external disturbances, then a regulator would not be needed to control the system. A measure of how well the used torque feed forward model is, could be made by looking at the control signal from the regulator when the torque feed forward was used. Doing a step trajectory with finite jerk, and plotting the torque reference from feed forward and the torque reference from the regulator, resulted in Figure 4.13.

Looking at Figure 4.13, it could be seen that the torque feed forward was lacking as the cart started moving and as the cart stopped, and that the regulator needed to compensate for this. Otherwise whilst following the trajectory, the control signal from the regulator seemed to have zero mean, meaning that the regulator did not need to work much.

Results from Figure 4.13 seemed satisfactory for this application, as the focus did not lie in optimising the torque model for the system, but rather investigating dual motor control.

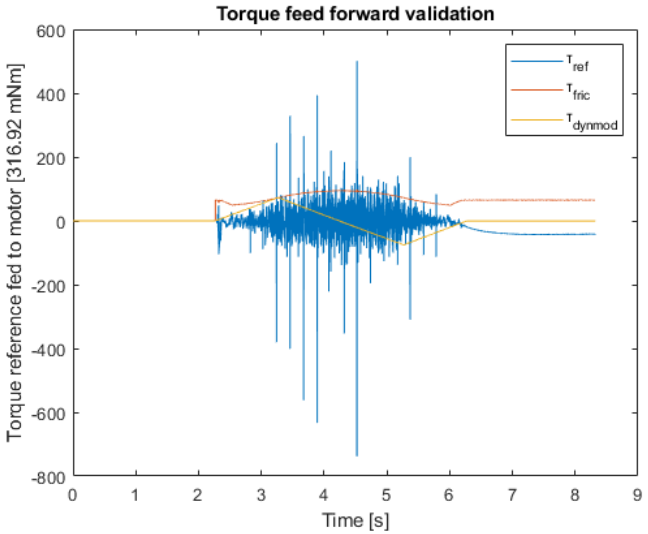

Figure 4.13 Control signal when using torque feed forward while following a step trajectory with finite jerk.

4.4 Single motor control

In the upcoming Chapter 5, only Motor 1 is used to control the cart position as Motor 2 is run in the opposite direction to close the backlash in the gear transmission. It was therefore critical to first evaluate tuning when only using one motor. This was done in this section.

For evaluating single motor control, the torque reference was set to zero for Motor 2, as Motor 2 being fed a torque could be seen as this situation but with disturbances from inertia. Performance was then evaluated from trajectories while using the same control structure as before, but where τ_{totref} was only fed to Motor 1.

Interestingly, the cart maintained its characteristics despite only using one motor. Velocity step responses as well as trajectory positioning seemed to be very similar as to when both motors were used. Because of this and for simplicity, the tuning for Motor 1 remained the same despite if Motor 2 was in torque control or regular control.

Static friction

In the following chapter, it is also of relevance to know the torque for static friction when only using one motor. Therefore, an experiment was conducted as follows.

While Motor 2 was fed with a torque reference of zero, Motor 1 was fed with a

torque reference which slowly increased. When the cart started moving, the torque reference for Motor 1 was noted. This process was repeated five times. The average of these torque references at which the cart started moving, was therefore a measure of the static friction when only using one motor.

Doing this experiment resulted in the static friction when only using one motor corresponding to $\tau_{m1/fric} = 143$ [316.92 mNm].

5

Control with backlash compensation

For control with backlash compensation, the control structure was as in Figure 5.1. The main difference was that the second motor was fed a different torque when the backlash compensation was active.

The backlash compensation consisted of a switching function, and a function which determined the sign of the torque fed to Motor 2.

5.1 Switching functions

It was desired for the cart to make a smooth transition between regular control, where both motors work identically, and when Motor 2 was fed a constant torque in a direction i.e., when Motor 2 was in torque control. This was done with a switching function. Torque fed to Motor 2, τ_{m2}, was according to Eq. (5.1)

$$\tau_{m2} = \tau_{totref}(1-\lambda|\operatorname{sign}_{trqctrl}|)+\lambda \operatorname{sign}_{trqctrl}\tau_{trqctrl}, \tag{5.1}$$

where $\lambda = [0,1]$ determined to which degree torque control was active, where $\lambda = 1$ meant full torque control and $\lambda = 0$ meant no torque control. $\tau_{trqctrl}$ [316.92 mNm] was the magnitude of the torque fed to Motor 2 in full torque control, and $\operatorname{sign}_{trqctrl}$ determined the desired sign of $\tau_{trqctrl}$.

In Eq. (5.1), note that Eq. (5.2) holds

$$\tau_{m2} = \begin{cases} \tau_{totref} & \text{if } \lambda = 0 \text{ or } \operatorname{sign}_{trqctrl} = 0 \\ \tau_{trqctrl} & \text{if } \lambda = 1 \text{ and } \operatorname{sign}_{trqctrl} = 1 \\ -\tau_{trqctrl} & \text{if } \lambda = 1 \text{ and } \operatorname{sign}_{trqctrl} = -1 \end{cases}. \tag{5.2}$$

When choosing $\tau_{trqctrl}$, it was important for it to be chosen large enough so that Motor 2 was fed with enough torque to be able to close the backlash gap. However, $\tau_{trqctrl}$ should also not be chosen too large as not to reduce too much performance

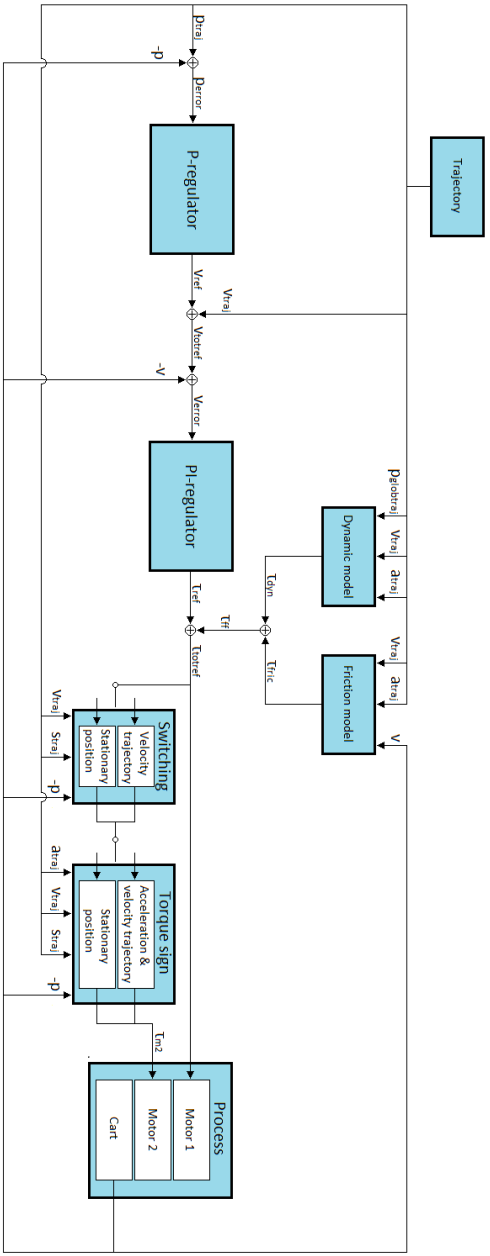

Figure 5.1 The control structure to be used with backlash compensation. Motor 2 was fed a new torque τ_{m2} [316.92 mNm].

of Motor 1. Therefore, it was chosen that Motor 2 was fed with torque according to the static friction when only using one motor i.e., $\tau_{trqctrl} = \tau_{m1/fric} = 143$ [316.92 mNm].

The following section presents two ways the switching variable λ could be determined.

Using the velocity trajectory

One way this could be done is by using the velocity trajectory v_{traj}. The switching variable using velocity trajectory, λ_v, could be determined according to Figure 5.2 and Eq. (5.3)

$$\lambda_v = \begin{cases} 0 & \text{if } |v_{traj}(k)| < \delta_{vmin} \\ \frac{|v_{traj}(k)| - \delta_{vmin}}{\delta_{vmax} - \delta_{vmin}} & \text{if } \delta_{vmin} \leq |v_{traj}(k)| < \delta_{vmax} \\ 1 & \text{if } \delta_{vmax} \leq |v_{traj}(k)| \end{cases}, \tag{5.3}$$

where δ_{vmax} [mm/s] > δ_{vmin} [mm/s] ≥ 0. For this master thesis, $\delta_{vmin} = 0$ mm/s was chosen because trajectories were used to trigger the switching function, which did not cause any oscillatory behaviour to be introduced into λ_v; $\delta_{vmax} = 1$ mm/s was also chosen, which resulted in a fast but not instantaneous switch to torque control when following trajectories.

Note that using λ_v resulted in permanent torque control whilst the trajectory was at a stationary position point.

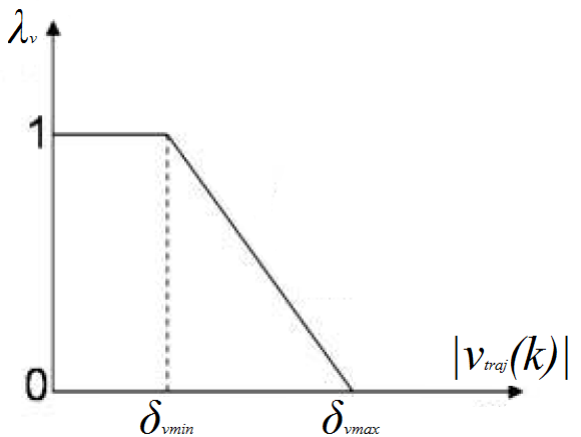

Figure 5.2 Switching variable using velocity trajectory.

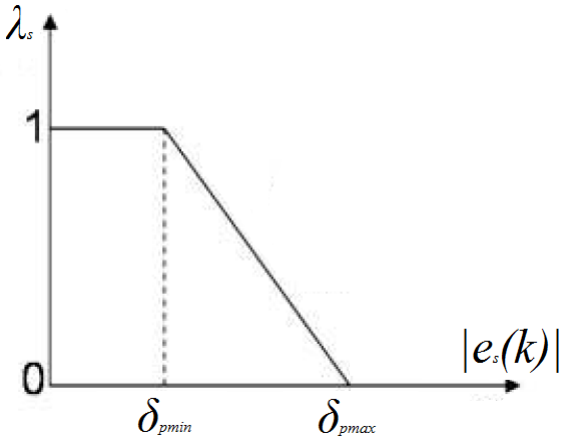

Figure 5.3 Switching variable using stationary position points.

Using stationary position points

Another way the switching variable could be determined was by using stationary position points given by s_{traj}. The switching variable using stationary position points, λ_s, could determined according to Figure 5.3 and Eq. (5.4)

$$\lambda_p = \begin{cases} 0 & \text{if } |e_s(k)| < \delta_{pmin} \\ \frac{|e_s(k)|-\delta_{pmin}}{\delta_{pmax}-\delta_{pmin}} & \text{if } \delta_{pmin} \leq |e_s(k)| < \delta_{pmax} \\ 1 & \text{if } \delta_{pmax} \leq |e_s(k)| \end{cases}, \tag{5.4}$$

where δ_{pmax} [mm] > δ_{pmin} [mm] ≥ 0. In this master thesis, it was chosen that $\delta_{pmax} = \delta_2$ and $\delta_{pmin} = \delta_1$, so that the friction model and λ_p were synchronised.

Using λ_s resulted in torque control relative to the current upcoming stationary position point. This allowed for Motor 2 to help control when the cart was subjected to external disturbances.

The idea of using position measurements to determine the switching variable was used in [Halt, 2009] and [Schiffer, 2009], and seemed to be a promising switching strategy.

5.2 Torque control sign functions

The purpose of the torque control sign function $\text{sign}_{trqctrl}$ was to determine the sign of the torque fed to Motor 2 in full torque control. In [Halt, 2009] and [Schiffer, 2009], $\text{sign}_{trqctrl}$ was chosen as the opposite of the velocity when approaching a stationary point. This seemed reasonable, as this made it so that Motor 1, which was

responsible for the primary position control, never had to travel across the backlash gap as it approached the stationary position point. Choosing $\text{sign}_{trqctrl}$ this way also probably made it so that the cart did not suffer from additional overshoot, but rather a more dampened response.

This section presents two ways the torque control sign function $\text{sign}_{trqctrl}$ could be determined.

Using the acceleration and velocity trajectory

One way this could be done was by using the acceleration and velocity trajectories a_{traj} and v_{traj}. The torque control sign function using acceleration and velocity trajectories, $\text{sign}_{trqctrl/av}$, could be according to Eq. (5.5)

$$\text{sign}_{trqctrl/av}(k) = \begin{cases} -1 & \text{if } v_{traj}(k) > \delta_v \text{ and } a_{traj}(k) < -\delta_a \\ 1 & \text{if } v_{traj}(k) < -\delta_v \text{ and } a_{traj}(k) > \delta_a \\ 0 & \text{if } v_{traj}(k) > \delta_v \text{ and } a_{traj}(k) > \delta_a \\ 0 & \text{if } v_{traj}(k) < -\delta_v \text{ and } a_{traj}(k) < -\delta_a \\ \text{sign}_{trqctrl/av}(k-1) & \text{otherwise} \end{cases}, \tag{5.5}$$

where δ_v [mm/s] and δ_a [mm/s^2] were very small values. For this master thesis, it was chosen that $\delta_v = 10^{-10}$ mm/s and $\delta_a = 10^{-10}$ mm/s^2.

Using $\text{sign}_{trqctrl/av}$ according to Eq. (5.5), resulted in the torque sign for Motor 2 to be in the opposite direction of the velocity, as the cart tried to reduce its absolute velocity. As the cart had reached a stationary point, then $\text{sign}_{trqctrl/av}$ remained the same. If it was desired for the cart to increase its absolute velocity, then $\text{sign}_{trqctrl/av}$ was set to zero, indicating that it was not desirable to use torque control.

Using stationary position points

Another way $\text{sign}_{trqctrl}$ could be determined was by using stationary position points given by s_{traj}. The torque control sign function using stationary position points, $\text{sign}_{trqctrl/s}$, could be according to Eq. (5.6)

$$\text{sign}_{trqctrl/s}(k) = \begin{cases} -1 & \text{if } e_s(k) > \delta_{pmin} \\ 1 & \text{if } e_s(k) < -\delta_{pmin} \\ \text{sign}_{trqctrl/s}(k-1) & \text{otherwise} \end{cases}. \tag{5.6}$$

Using $\text{sign}_{trqctrl/s}$ according to Eq. (5.6), resulted in the torque sign for Motor 2 to be in the opposite direction of the velocity when approaching a stationary position point, given that there was no torque control before the approach. This allowed for $\text{sign}_{trqctrl/s}$ to adapt to external disturbances.

Due to $\text{sign}_{trqctrl/s}$ adapting to external disturbances, then it was probably not a good idea to use this together with λ_v, as λ_v did not do this.

6

Experimental evaluation

In this section, an experimental evaluation was made regarding position accuracy with and without external disturbances. The experimental evaluations were made using different methods to obtain λ and $\text{sign}_{trqctrl}$. It was also investigated how the motors traversed through the backlash gap when subjected to an external disturbance.

6.1 Position accuracy without external disturbances

Here are results from a position accuracy evaluation without external disturbances presented. The evaluation consisted of a limit cycle analysis and a position accuracy comparison using both a step with finite jerk and a cosine trajectory.

Limit cycles

In Figure 6.1, a plot can be seen for measured cart position p with the position reference p_{ref} set to zero. Results can be seen when the cart was in either regular control or in full torque control.

Looking at Figure 6.1, effects of limit cycles could be seen for the case when the cart was in regular control, and these were removed when the cart was in full torque control. The effects of the limit cycles were however surprisingly small, and seem irregular.

A reason for this may be due to the presence of the second motor. The second motor added more friction to the system. Another reason for this may be that the position in the gaps were not synchronised, making so that the limit cycles for each motor were also not synchronised, resulting in a smaller, more irregular pattern for the position measurement. To confirm this however, a limit cycle analysis for each motor individually should be made.

Step trajectory with finite jerk

In this evaluation, a trajectory was used for taking a step with finite jerk together with different methods to obtain λ and $\text{sign}_{trqctrl}$. The absolute error for position

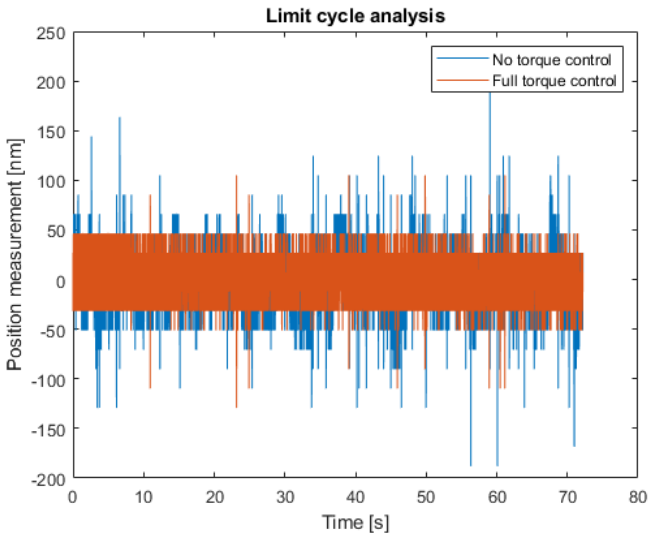

Figure 6.1 Position measurements when the position reference is set to zero.

data was then integrated at the region where the switching functions were active. The integrated absolute error was then normalised relative to the case where no backlash compensation was active.

Letting the cart follow a step trajectory with finite jerk with different methods to obtain λ and $\text{sign}_{trqctrl}$, in the region where the switching variables are active, can be seen in Figure 6.2. The normalised integrated absolute error in Figure 6.2 can be seen in Figure 6.3.

Looking at Figure 6.2, it could be seen that using no backlash compensation resulted in the fastest response with a settling time of around 1 s, but also with an overshoot. However, looking at the very small scale, it can be seen that this overshoot was about 10^{-2} of the magnitude of the backlash position errors Δp_1 and Δp_2. Using λ_s resulted in a more damped response with no overshoot but also with a larger settling time of about 3 s. However, signs of instability appeared as λ_s was applied. Using either $\text{sign}_{trqctrl/av}$ or $\text{sign}_{trqctrl/s}$ did not seem to matter much in this case as $\text{sign}_{trqctrl}$ never changed value i.e., that there was never an absolute overshoot larger than δ_{pmax}. However, using λ_v did not seem to result in good performance for this experiment. There was a large settling time of about 7 s and an overshoot. The cart was also very quickly pushed back as torque control started using λ_v.

Looking at Figure 6.3, it was summarised that no compensation resulted in the best position accuracy using a step trajectory, followed by using λ_s and lastly by using λ_v.

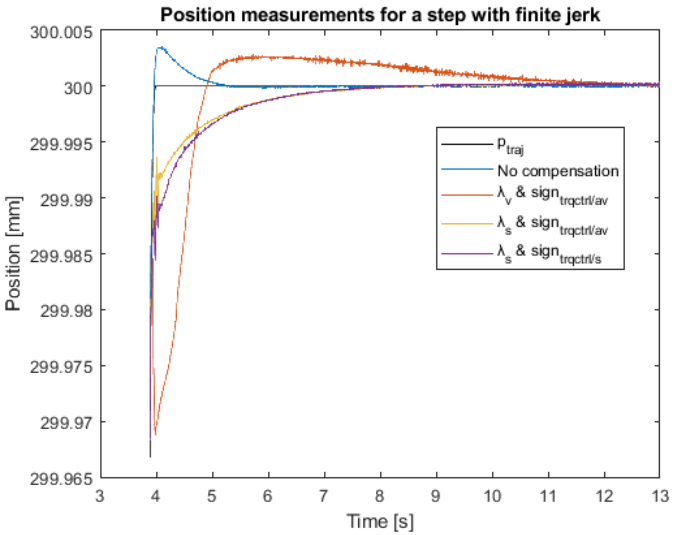

Figure 6.2 Step trajectory with finite jerk, where $j_{max} = 300$ mm/s^3, $a_{max} = 200$ mm/s^2, $v_{max} = 200$ mm/s and $p_f = 300$ mm. Different methods were used to obtain λ and sign$_{trqctrl}$.

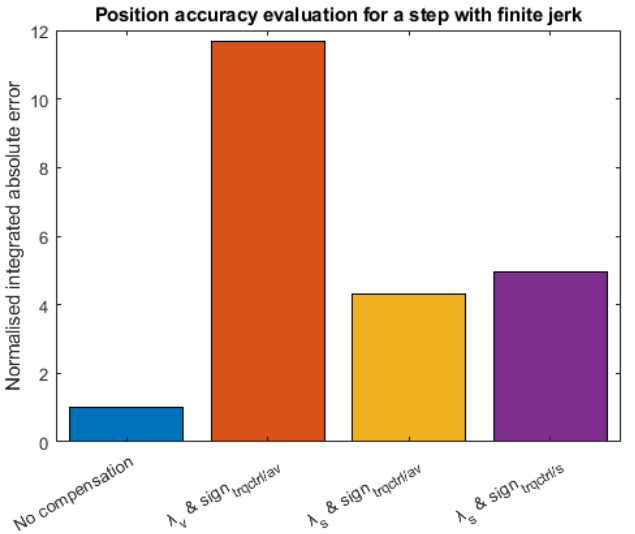

Figure 6.3 Integrated absolute position error in Figure 6.2, and normalised against the case with no backlash compensation.

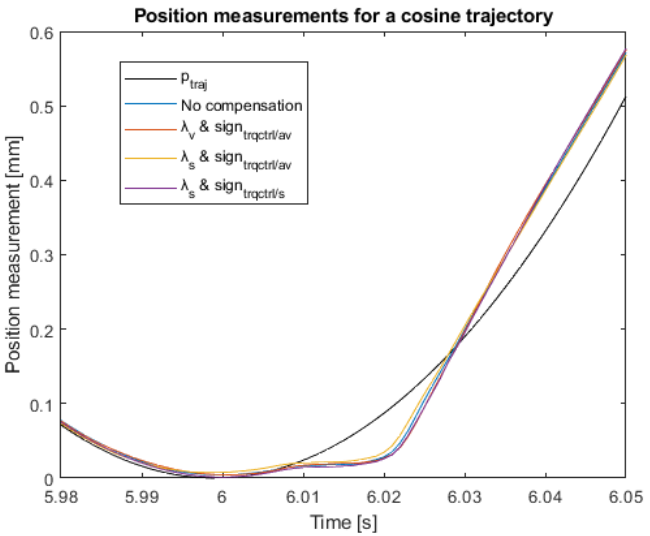

Figure 6.4 Cosine trajectory with $A_{cos} = 90$ mm and $T_{cos} = 3$ s for different methods to obtain λ and $\text{sign}_{trqctrl}$, in the region where the switching variables activate.

Cosine trajectory

In this evaluation, it was investigated how the backlash compensation affected more dynamic trajectories, such as the cosine trajectory. The experiment was made by letting the cart follow a cosine trajectory with different methods to obtain λ and $\text{sign}_{trqctrl}$, and investigating the position accuracy around a region where the switching functions were active.

Results from this experiment can be seen in Figure 6.4, and the normalised integrated absolute error in Figure 6.4 can be seen in Figure 6.5.

Looking at Figure 6.4, it could be seen that using backlash compensation did not seem to have any significant impact on the position accuracy when evaluating more dynamic trajectories. This could also be summarised by Figure 6.5. The more interesting aspect of Figure 6.4 may rather be the shortcomings of the friction model.

6.2 Position accuracy with external disturbances

In this section, an evaluation of performance was made when the cart was subjected to an external disturbance $F_D = 140$ N. First, an evaluation regarding position overshoot and settling time was made, followed by an analysis of the backlash traversal. The experiments were made with different methods of calculating λ and $\text{sign}_{trqctrl}$ as well as different signs of the initial torque fed to Motor 2. The sign of the initial

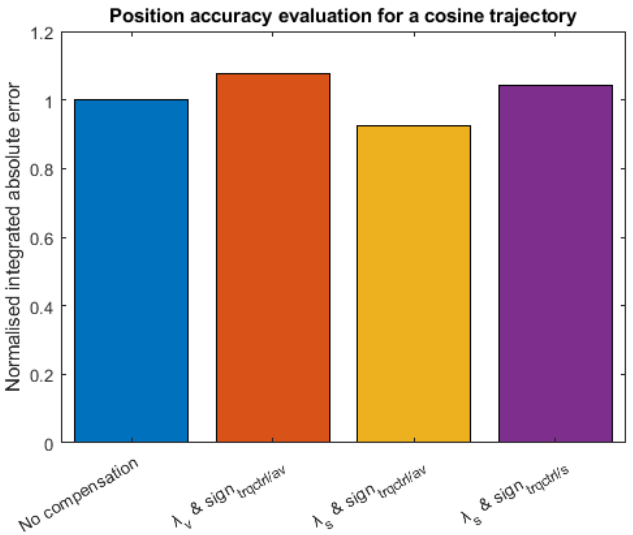

Figure 6.5 Integrated absolute position error in Figure 6.4, and normalised against the case with no backlash compensation.

torque fed to Motor 2 was denoted $\text{sign}(\tau_{m2}(0))$.

Overshoot and settling time

An evaluation regarding overshoot and settling time was made as follows.

The cart first followed a step trajectory where the cart had its final destination reached as well as the system having entered stationarity. The cart was then subjected to a step disturbance $F_D = 140$ N, by hanging a weight to the cart. After the cart had reached stationarity, the weight was then removed. The cart was then allowed to enter stationarity again. Throughout the process, the maximum position error and settling time was noted. The settling time for this experiment was defined as when the position had settled within 10^{-4} mm from the position reference. For each case, the experiment was repeated three times, as the method of manually attaching a weight to the cart did not result in good repeatability in obtained data. The mean of these three experiments would then serve as the results from that specific case.

Results from doing these experiments can be seen in Figures 6.6 and 6.7.

Looking at Figure 6.6, it could be seen that using no compensation seemed to in general yield the best results for this experiment, except for the case when F_D was applied and $\text{sign}(\tau_{m2}(0)) = \text{sign}(F_D)$ (blue). For this case, the results seemed to coincide with stiffness experiments done in [Halt, 2009], where using λ_v was better than not using any compensation, but using λ_s resulted in the best results. Also note

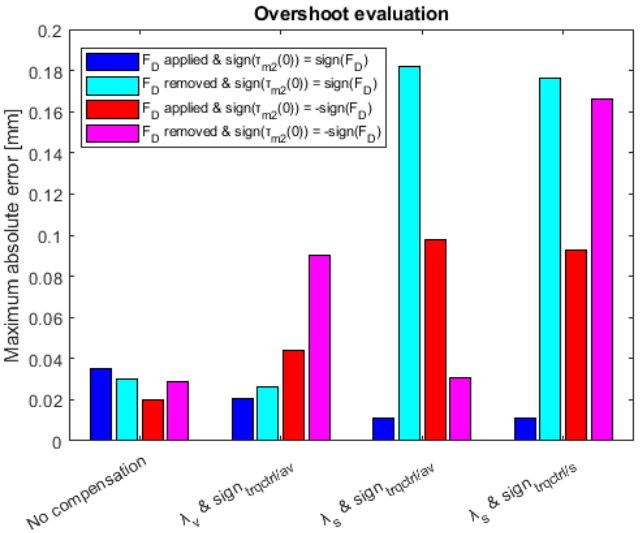

Figure 6.6 Maximum position error when the cart is subjected to a step disturbance for different control settings.

the small scale of the overshoots, which were about 10^{-1} of the magnitude of the backlash position errors Δp_1 and Δp_2.

When using λ_v, performance seemed much worse for $\text{sign}(\tau_{m2}(0)) = -\text{sign}(F_D)$ (red and magenta) compared to when no backlash compensation was used.

However when using λ_s, the cart seemed to have large overshoots for most other cases, except when $\text{sign}_{trqctrl/av}$ was used for the case when F_D was removed and $\text{sign}(\tau_{m2}(0)) = -\text{sign}(F_D)$ (magenta).

According to this overshoot analysis, using no compensation yielded the overall best results, but using λ_v and λ_s together with $\text{sign}_{trqctrl/av}$ could be promising if their shortcomings are dealt with. The most promising of these may be when using λ_s and $\text{sign}_{trqctrl/av}$.

Instead looking at Figure 6.7, it could be seen that in general the lowest settling times were when not using any backlash compensation. This makes sense as both motors were able to be used to bring the cart back to the reference.

The settling times for when using λ_s for the case when F_D was applied and $\text{sign}(\tau_{m2}(0)) = \text{sign}(F_D)$ (blue) seemed to be similar to when no compensation was used. However using λ_v seemed to increase the settling time for this case.

For the case when F_D was removed and $\text{sign}(\tau_{m2}) = \text{sign}(F_D)$ (cyan), using λ_s with $\text{sign}_{trqctrl/av}$ seemed to give a similar settling time as when no compensation was used. Using λ_s and $\text{sign}_{trqctrl/s}$ seemed result in the highest settling time for this

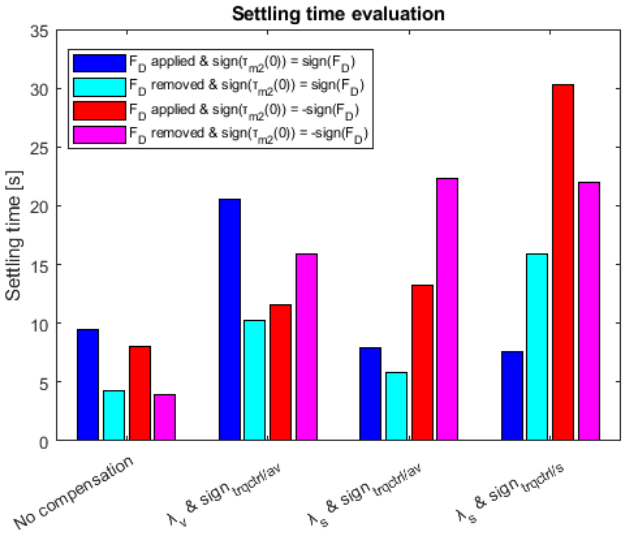

Figure 6.7 Settling time when the cart was subjected to a step disturbance for different control settings.

case.

For the case when F_D was applied and $\text{sign}(\tau_{m2}) = -\text{sign}(F_D)$ (red), using any compensation resulted in a larger settling time compared to not using any compensation. Using λ_s together with $\text{sign}_{trqctrl/s}$ seemed to result in a very large settling time.

For the case when F_D was removed and $\text{sign}(\tau_{m2}) = -\text{sign}(F_D)$ (magent), using any compensation resulted in a greatly increased settling time.

According to this settling time analysis, it was concluded that using no compensation yielded the best overall results.

Backlash traversal

This section aims to investigate the backlash traversal for the different cases presented in the overshoot and settling time analysis. This was done by looking at the difference in measurements from the linear encoder on the cart and the rotary encoders in the motors. An experiment was conducted as follows.

When the cart had entered stationarity after having reached its final destination from a step trajectory, then the difference in measurements from the linear and rotary encoders were reset to zero. The difference from the encoders, λ and $\text{sign}_{trqctrl}$ were recorded while the disturbance F_D was both applied and removed. This gave information on where the motors were in the backlash gap, because when the encoder difference lay within a close proximity of zero, it could be assumed that the

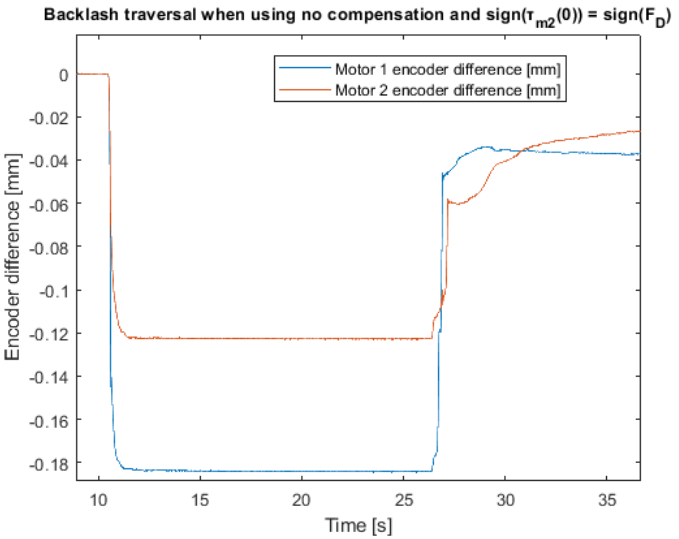

Figure 6.8 Encoder differences when F_D was applied and removed when using no compensation and $\text{sign}(\tau_{m2}(0)) = \text{sign}(F_D)$.

position in the gap was the same as in the beginning of the experiment. However, if the absolute encoder difference was within the size of Δp_1 and Δp_2, then it could be assumed that the respective motors lay on the opposite side of the gap as when the experiment started.

Results from these experiments for the different cases are presented in the following subsections.

Using no compensation and $sign(\tau_{m2}(0)) = sign(F_D)$ Looking at Figure 6.8, it can be seen that both motors have traversed through the backlash gap once F_D was applied.

When F_D was removed, the cart made an overshoot, making the motors having to go through the backlash gap once again. At the endpoint, the motors ended up in an arbitrary position in the gap due to them not going in different directions.

Using no compensation and $sign(\tau_{m2}(0)) = -sign(F_D)$ Looking at Figure 6.9, it could be seen that both motors traversed partly through the backlash gap when F_D was applied. This was probably due to the cart already partly being on the right side of the gap before F_D was applied.

When F_D was removed, both motors had to go through the backlash gap again and ended up in an arbitrary position in the gap due to them not going in different directions.

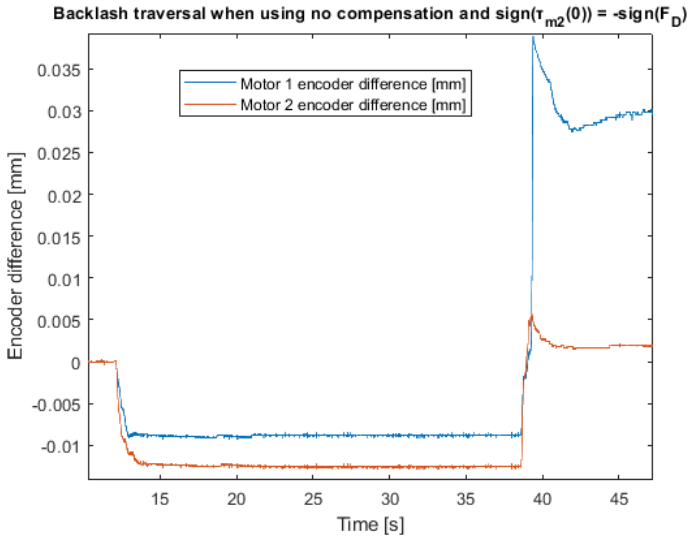

Figure 6.9 Encoder differences when F_D was applied and removed when using no compensation and $\text{sign}(\tau_{m2}(0)) = -\text{sign}(F_D)$.

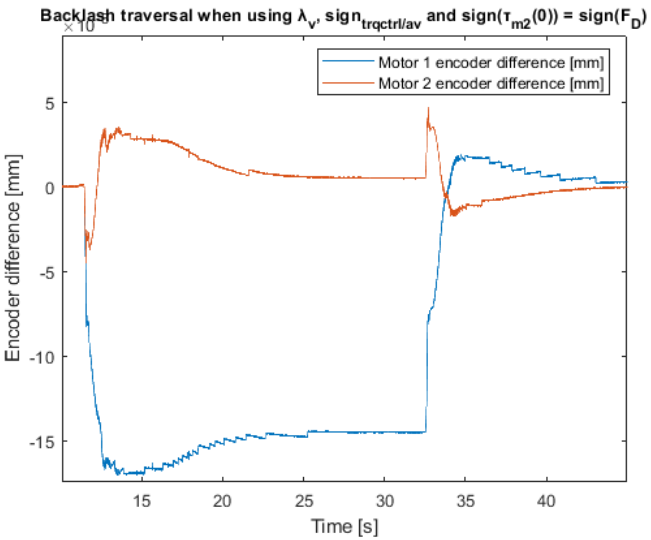

Figure 6.10 Encoder differences when F_D was applied and removed when using λ_v, $\text{sign}_{trqctrl/av}$ and $\text{sign}(\tau_{m2}(0)) = \text{sign}(F_D)$.

Using λ_v***,*** $sign_{trqctrl/av}$ ***and*** $sign(\tau_{m2}(0)) = sign(F_D)$ Looking at Figure 6.10, it could be seen that neither motor went through the whole backlash gap when F_D was applied. It could however be seen that Motor 2 briefly started going through the backlash gap, but then gained contact again.

The Motor 1 encoder difference differed from zero after F_D had been applied. This may be due to Motor 1 having to increase its torque against the disturbance, which maybe resulted in elastic deformation.

Interestingly when F_D was removed, Motor 1 did not seem to go through the backlash gap. This would be expected as Motor 1 would need to change direction to get the cart back to its original position due to the overshoot when F_D was removed. One explanation to this may be that Motor 2 instead took the cart back to its original position as Motor 1 very briefly did not remain in contact when F_D was removed. Evidence of Motor 2 very briefly pushing the cart itself, could be the small peak when F_D was removed, which indicates elastic deformation of the gear because of it suddenly being in contact with the rail. This may be the reason for the increased overshoot when F_D was removed, compared to the case with no compensation.

Using λ_v***,*** $sign_{trqctrl/av}$ ***and*** $sign(\tau_{m2}(0)) = -sign(F_D)$ Looking at Figure 6.11, it could be seen that Motor 1 went through the backlash gap when F_D was applied. For Motor 2, a small dip was followed by a small spike as F_D was applied. The small dip may be from when the cart moved due to F_D, while Motor 1 still has not had the time to travel in the backlash gap to respond. Only Motor 2 should be in contact

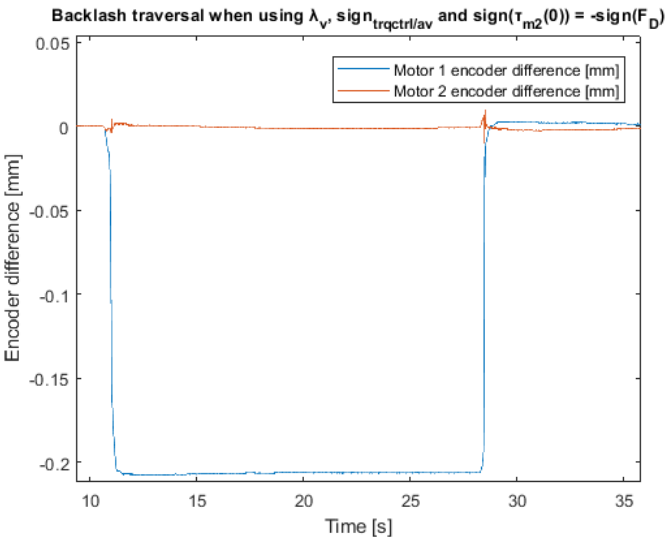

Figure 6.11 Encoder differences when F_D was applied and removed when using λ_v, $\text{sign}_{trqctrl/av}$ and $\text{sign}(\tau_{m2}(0)) = -\text{sign}(F_D)$.

here. Since the cart started moving in the opposite direction as Motor 2, then this would result in Motor 2 having less force pushed on the gear for this brief moment, which may have resulted in the dip. The small spike may then be when Motor 1 had travelled through the backlash gap and gained contact on the other side. For a brief moment, then the force on the gears for Motor 2 would increase, which may result in the spike.

When F_D was removed, it could be seen that Motor 1 travelled through the backlash gap again. For a brief moment, the encoder difference increased before it rapidly went to zero. This may be due to the force on the gears for Motor 1 being reduced as F_D was removed, making the cart overshoot. For Motor 2, when F_D was removed, a peak followed by an alternating spike could be seen. The peak may be from when Motor 1 pushed the cart away from the position reference, and when Motor 1 had not yet had the time to compensate for the removal of F_D. The alternating spike for Motor 2 may have been from when Motor 1 moved through the backlash gap and gained contact on the other side.

Using λ_s***,*** $sign_{trqctrl/av}$ ***and*** $sign(\tau_{m2}(0)) = sign(F_D)$ Looking at Figure 6.12, it could be seen that Motor 1 did not go through the backlash gap when F_D was applied. It could also be seen that Motor 2 slowly started to transition to regular control and that Motor 2 started moving in the gap to help Motor 1. This was probably the reason for the very low overshoot.

However, when F_D was removed, then Motor 1 needed to travel through the

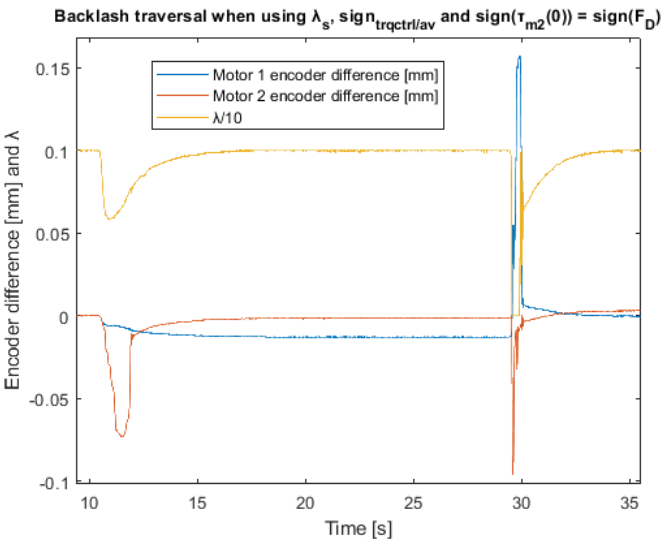

Figure 6.12 Encoder differences when F_D was applied and removed when using λ_s, $\text{sign}_{trqctrl/av}$ and $\text{sign}(\tau_{m2}(0)) = \text{sign}(F_D)$.

backlash gap to compensate for this. When Motor 1 had travelled through the backlash gap, made it so that Motor 2 transitioned to full regular control as well due to the position overshoot. This made it so that both motors initially had to go through the backlash gap when F_D was removed.

When the cart approached the position reference after F_D had been removed, then torque control started for Motor 2, making Motor 2 going through the backlash gap again. To compensate for this, Motor 1 needed to go through the gap once again to hold against Motor 2. Because both motors went through the backlash gap twice may be the reason for the large overshoot when F_D was removed.

Using λ_s***,*** $sign_{trqctrl/av}$ ***and*** $sign(\tau_{m2}(0)) = -sign(F_D)$ Looking at Figure 6.13 when F_D was applied, then it looked strikingly similar to when λ_v was used in Figure 6.11. The only difference may be the dip for Motor 2 after the sharp peak. This may be due to Motor 2 being in regular control here, as seen by λ.

When F_D was removed, the brief moment when the cart made an overshoot could be seen for Motor 1, as the encoder difference became slightly larger before Motor 1 closed the backlash gap again. It could also be seen that Motor 2 transitioned to almost full regular control to help Motor 1.

Using λ_s***,*** $sign_{trqctrl/s}$ ***and*** $sign(\tau_{m2}(0)) = sign(F_D)$ Looking at Figure 6.14 when F_D was applied, then it looked strikingly similar to when λ_s and $\text{sign}_{trqctrl/av}$ were used in Figure 6.12. Looking at $\text{sign}_{trqctrl}$, since it did not change as F_D was ap-

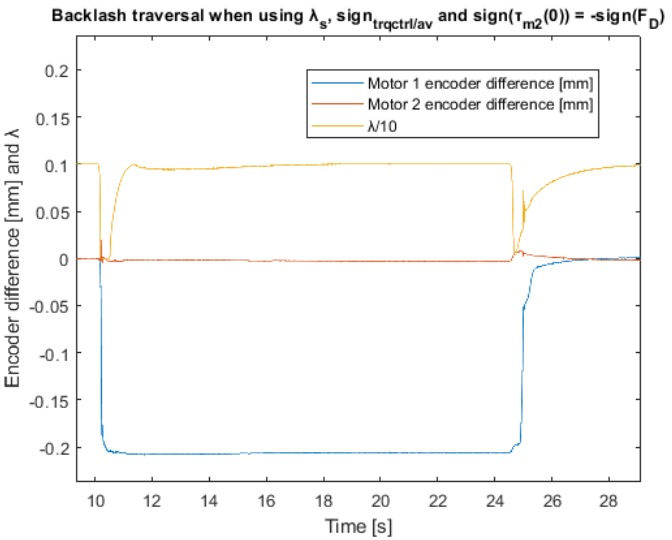

Figure 6.13 Encoder differences when F_D was applied and removed when using λ_s, $\text{sign}_{trqctrl/av}$ and $\text{sign}(\tau_{m2}(0)) = -\text{sign}(F_D)$.

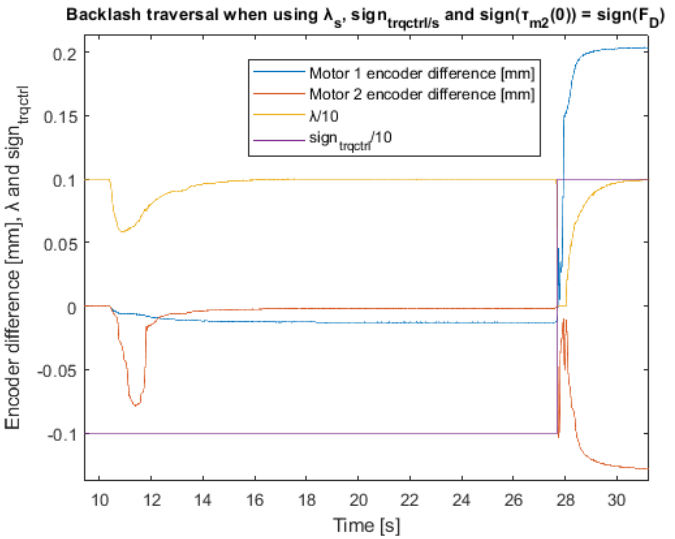

Figure 6.14 Encoder differences when F_D was applied and removed when using λ_s, $\text{sign}_{trqctrl/av}$ and $\text{sign}(\tau_{m2}(0)) = \text{sign}(F_D)$.

plied, then it these two cases would be identical here. This could also be seen in the overshoot and settling time analysis.

Initially when F_D was removed and $\text{sign}_{trqctrl/s}$ had not changed yet, then Figure 6.14 looked very similar to when λ_s and $\text{sign}_{trqctrl/av}$ were used in Figure 6.12. The difference was that $\text{sign}_{trqctrl}$ changed, making it so that the final torque control ended up with the Motor 2 torque being in the opposite direction as in the beginning. This change made it so that both motors ideally would not have to travel back through the backlash gap as the cart entered torque control again. There still seemed to be complications present as seen by the spikes when F_D was removed. Looking at the overshoot analysis in Figure 6.6, then the overshoot for this case (cyan) remained the same as when $\text{sign}_{trqctrl/av}$. Using $\text{sign}_{trqctrl/s}$ instead of $\text{sign}_{trqctrl/av}$ also increased the settling time as seen in Figure 6.7.

Using λ_s, $sign_{trqctrl/s}$ ***and*** $sign(\tau_{m2}(0)) = -sign(F_D)$ Looking at Figure 6.15 when F_D was applied, then it looked very similar to when λ_s and $\text{sign}_{trqctrl/av}$ were used in Figure 6.11. However after the initial overshoot, $\text{sign}_{trqctrl}$ changed so that Motor 2 instead lay on the opposite side of the gap while F_D was still applied to the cart. Using $\text{sign}_{trqctrl/s}$ instead of $\text{sign}_{trqctrl/av}$ resulted in a larger settling time as seen in Figure 6.7 for this case (red).

When F_D was removed, both motors went through the backlash gap again, and $\text{sign}_{trqctrl}$ changed once again. The ripples for Motor 2 may be a combination of Motor 2 helping Motor 1, and also when only Motor 2 had contact while Motor 1

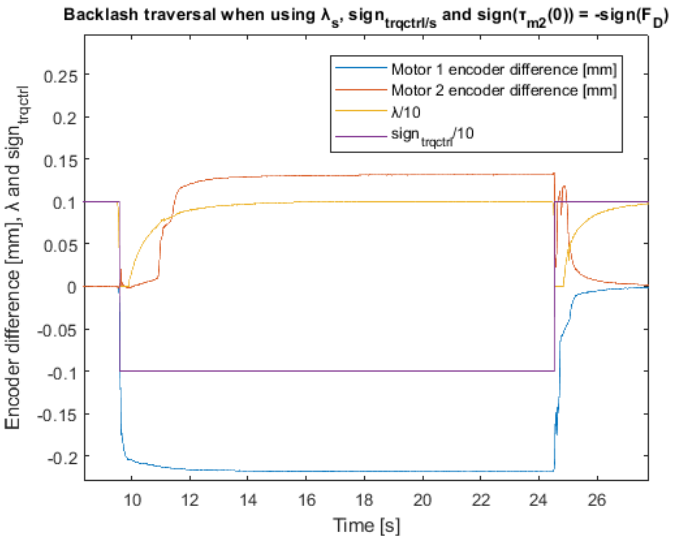

Figure 6.15 Encoder differences when F_D was applied and removed when using λ_s, $\text{sign}_{trqctrl/av}$ and $\text{sign}(\tau_{m2}(0)) = -\text{sign}(F_D)$.

went through the backlash gap. After F_D had been removed, then both motors ended up on the same side of the backlash gap as before F_D was applied. Using $\text{sign}_{trqctrl/s}$ instead of $\text{sign}_{trqctrl/av}$ resulted in a larger overshoot as seen in Figure 6.6 for this case (magenta).

Summary of backlash traversal Looking at the backlash traversal, a contributing factor for large overshoots may have been because Motor 1 travelled through the backlash gap, despite Motor 2 having contract. The cases where $\text{sign}_{trqctrl/s}$ was used and it changed value, resulted in worse performance in comparison to using $\text{sign}_{trqctrl/av}$.

7

Discussion

The torque feed forward used in this master thesis came from simplified models which modelled known phenomena of the system. These models are in need of further improvements as seen in Figure 4.13, where the torque feed forward was lacking around position stationarity. The magnitude of the friction model could for example be improved by introducing dynamic friction and temperature dependence, and the sign of the friction model could need further improvements around position stationarity. Special attention could also be made in either the friction model or dynamic model regarding the launch of the cart, as the small spikes in the torque data seen in Figure 4.13 were not modelled as the cart started moving.

Interesting dynamics seemed to appear for the stationary torque required to maintain a constant velocity, seen in Figure 4.3. One reason for this may have been because of dynamics of the servo motors themselves. Another reason for this may have been because of the varying sizes of the backlash gap across the rail.

As seen in Figure 6.2, there was a very small position overshoot for the case when no backlash compensation was used. The overshoot was however very small, and was about 10^{-2} of the magnitude of the backlash position errors Δp_1 and Δp_2. Worth noting is that the overshoot was small enough for the motors not having to travel through the backlash gap after the position overshoot. It was sufficient for the control signal to decrease to make it so that the cart position went back to the position reference.

Plenty of possible solutions were evaluated to see if this position overshoot could be eliminated. One such solution was to remove overshoots for velocity step responses at low velocities, which may have been the most likely reason for the position overshoot. However, as mentioned before, none of the investigated velocity controllers seemed to give satisfactory results. The simple PI-regulator was therefore chosen to control the velocity, as it seemed to have the least amount of drawbacks.

Another solution which was evaluated to see if the position overshoot could be eliminated, was to re-tune the control parameters K_p, K_v and $K_{i/v}$. The most promising way to remove position overshoot may have been to increase K_v, as it worked as derivative gain for the position control, meaning that an increase in K_v would

yield more dampened position control. The velocity was however derived from differentiation, resulting in introduced signal noise. Increasing K_v did not result in the position overshoot being removed, but rather introduced more noise into the control signal.

Another solution which was evaluated was to remove Polynomial 1 in Figure 4.4 in the magnitude of the friction model as a stationary position point was approached. However, the position overshoot remained the same.

The sign of the friction model also underwent much iteration. The chosen sign function for the friction model was to have the same sign as the velocity trajectory, and to preserve the sign of the friction model as the current velocity trajectory was very small in magnitude. Using this sign function resulted in the least amount of drawbacks among other investigated alternatives. Using a sign function for the friction like this resulted in the friction model being active as a stationary position point had been reached, which for example resulted in large mismatches between the torque data and torque estimate for the dynamic model seen in Figure 4.12.

Another promising way the sign of the friction model could have been determined by was by using stationary position points seen in Figure 4.5. Using this sign function for the friction model resulted in very good position accuracy without any external disturbances present. The position overshoot was managed to be eliminated as well. Using this sign function would also make it so that the friction model would help when external disturbances were present. In reality, it was observed that large limit cycles could be introduced instead when external disturbances were present.

Other experiments made regarding the sign of the friction model were to have the sign function according to Figure 4.5, but using either v_{traj} or v_{totref} instead of e_s. This made it so that the friction model was turned off very early as stationary positions points were approached, which resulted in poor position accuracy without external disturbances.

To improve position control further, then it could also be experimented with to alter the system more during torque control. Tuning could for example be altered for the primary motor, and additional torque could be fed to the primary motor to compensate for the secondary motor going into torque control. The torque feed forward from the friction and dynamic model could also be incorporated into the switching.

The method for evaluating performance when external disturbances were present was also lacking. Only one weight was used, which possibly made it so that other relevant dynamics of the system were not observed. Manually applying the weight did also not result in good repeatability of measured data. Using a step disturbance may also not have been ideal to evaluate performance of the system, as using a step disturbance could excite mechanical resonances of the system.

Looking at the overshoot analysis seen in Figure 6.6, it could be seen that the overshoots using no compensation were only about 10^{-1} of the magnitude of the backlash position errors Δp_1 and Δp_2. It would therefore be interesting to evaluate performance where overshoots were large enough to leave the position region where

the switching parameters were active.

Using a weight to evaluate performance with external disturbances was a consequence of time frame and available resources. It would for example be interesting to evaluate stiffness of the cart position control, or to use larger, smoother and more repeatable external disturbances. An interesting stiffness evaluation was for example made in [Halt, 2009], where stiffness of the cart was evaluated using a force sensor.

8

Conclusion

Experiments showed that position accuracy could be maintained with a more dampened response when backlash compensation was active when no external disturbances were present. With external disturbances, low overshoot could be achieved for some situations when using the backlash-compensation methods, where results seemed to coincide with previous work. However, this came at a cost of higher overshoots for other situations, where the backlash-traversal analysis indicated that this may have been due to the controlling motor not being in contact. Experiments also showed that settling times were generally increased with backlash compensation, as only one motor was used when the backlash compensation was active.

From the experiments conducted in this master thesis, it was concluded that using no compensation yielded the best overall results. However, using a switching variable λ based on stationary position points and using a sign function for torque control $\text{sign}_{trqctrl}$ based on velocity- and acceleration trajectories seemed promising, but cases where the controlling motor went through the backlash would need to be addressed.

Things to consider may be that the velocity control was not ideal, as there were still overshoots when evaluating velocity step responses with low velocity references. The torque feed forward was also lacking, as the regulator had to work for low velocities, despite no external disturbances being present. Torque feed forward was also only done with data from regular control. The experiment by manually attaching a weight to attain an external step disturbance may also not be ideal, as the repeatability of the experiment was not good, and that mechanical resonances could be excited in the system. Only a single weight was used, so other relevant dynamics of the system may be yet to be seen with other weights.

8.1 Outlook

Possible future work may be as follows.

- Do more testing with the joint using external disturbances. An example may be to use smooth, repeatable forces with a large variety in magnitudes. An ex-

ternal force sensor can also be implemented to do more sophisticated stiffness experiments as in [Halt, 2009].

- Investigate methods to make it so that the controlling motor does not lose contact for some situations with external disturbances.
- Improve the control structure. Overshoots for low velocity step responses need to be dealt with, without compromising compensation for external disturbances.
- Improve the torque feed forward model, mainly as when the cart both launches from and arrives to position stationarity. Further investigations regarding torque feed forward in torque control could also be made.

Bibliography

Cairén, P. (2013). *Position Accuracy with Dual Motor Control for a Gantry-Tau Robot*. Master's Thesis ISRN LUTFD2/TFRT--5913--SE. Department of Automatic Control, Lund University, Lund, Sweden.

Hägglund, T. (2015). *Automatic Control Basic Course, Lectures*. Department of Automatic Control, Lund University, Lund, Sweden.

Halt, L. (2009). *Implementation and Evaluation of Accurate and Stiff Position Control for a Parallel Kinematic Robot*. Institute of Automatic Control, Department of Computer Science, Faculty of Electrical Engineering and Information Technology, Lund University, Darmstadt University of Technology, Lund, Darmstadt, Sweden, Germany.

Linderoth, M. (2013). *On Robotic Work-Space Sensing and Control*. PhD thesis TFRT-1098. Department of Automatic Control, Lund University, Lund, Sweden.

Marquez, F. and G. Domingues (2010). *DC Motor and Control*. Applied Mechatronics (EIEN45), Department of Industrial Electrical Engineering and Automation, Lund University, Lund, Sweden.

MathWorks (2019a). *Least-squares fitting*. URL: `https://se.mathworks.com/help/curvefit/least-squares-fitting.html` (visited on 2019-02-14).

MathWorks (2019b). *Signal smoothing*. URL: `https://se.mathworks.com/help/signal/examples/signal-smoothing.html` (visited on 2019-02-22).

Schiffer, J. (2009). *Dual motor control for backlash reduction*. Master's Thesis TFRT-5841. Department of Automatic Control, Lund University, Lund, Sweden.

SMErobot (2009). *Gantry-tau robot*. URL: `http://www.smerobot.org/` (visited on 2019-04-10).

Lund University
Department of Automatic Control
Box 118
SE-221 00 Lund Sweden

Document name
MASTER'S THESIS

Date of issue
June 2019

Document Number
TFRT-6086

Author(s)
Mathias Artursson

Supervisor
Olof Sörnmo, Cognibotics
Anders Robertsson, Dept. of Automatic Control, Lund University, Sweden
Rolf Johansson, Dept. of Automatic Control, Lund University, Sweden (examiner)

Title and subtitle
Dual-Motor Control for Backlash Reduction in Parallel-Kinematic Robot Joints

Abstract
A new high-performance robot called the Gantry-Tau robot was developed by ABB Robotics, the Robotics Lab at Lund University and Güdel AG. This robot seemed promising in terms of speed, accuracy, stiffness and bandwidth of the motion control. However, the robot joints were based on the rack-and-pinion principle, which introduced significant backlash into the system. To solve this problem, it was proposed to use two motors to control each joint, where the motors would go in opposite directions to ensure that the gears and motors were in contact at all times. How this should be implemented is still under development.

This master thesis attempted to implement backlash compensation together with conventional uses of the robot joints, such as position-, velocity- and accelerationtrajectories as well as torque feed forward. The goal for the cart was to have regular control for both motors when following trajectories, except for stationary points where the motors would work in different directions. A test rack was provided for this purpose by Lund University and Cognibotics.

First, trajectories were generated for the robot joint to follow. A control structure was then implemented for the robot joint, consisting of a cascade structure for position control, as well as torque feed forward from a friction and dynamic model. Different methods for backlash-compensation were also presented and implemented. These methods for backlash-compensation together with the control structure were then evaluated in terms of position accuracy without external disturbances, and overshoot, settling time and backlash traversal with external disturbances.

It was concluded that some implemented backlash compensation methods resulted in a more dampened response when no external disturbances were present. Experiments with external disturbances showed that performance could be improved in some situation, but became worse in others. The reason for this decreased performance may have been because the controlling motor went through the backlash gap.

Keywords

Classification system and/or index terms (if any)

Supplementary bibliographical information

ISSN and key title
0280-5316

ISBN

Language
English

Number of pages
1-82

Recipient's notes

Security classification

http://www.control.lth.se/publications/